*for submission to the AMERICAN JOURNAL OF SCIENCE*

April 4, 2002

# SPATIAL PATTERN OF EROSION IN THE GREAT SMOKY MOUNTAINS, NORTH CAROLINA AND TENNESSEE: IMPLICATIONS ON STEADY STATE MOUNTAIN BELTS

MATMON, A., BIERMAN, P. R., LARSEN, J., Geology Department, University of Vermont, Burlington, VT 05405

SOUTHWORTH, S., PAVICH, M., United States Geological Survey, Reston, VA 20192

FINKEL, R., CAFFEE, M.,* Lawrence Livermore National Laboratory, Livermore, CA 94550

* Current address: Prime Laboratory, Physics Department, Purdue University, West Lafayette, IN 47907

**ABSTRACT. Spatially homogeneous erosion rates of 25-30 m $My^{-1}$ prevail throughout the Great Smoky Mountains. $^{10}Be$ and $^{26}Al$ activities from sediments collected from headwater tributaries indicate an average erosion rate of 27±7 m $My^{-1}$, similar to that of the outlet rivers (24±6 m $My^{-1}$) that carry most of the sediment out of the mountain range. Analysis of $^{10}Be$ and $^{26}Al$ in bedrock, colluviall, and alluvial sediments, coupled with field observations and GIS study suggest that erosion in the Great Smoky Mountains is controlled by slope diffusive processes. The results indicate rapid alluvial transport and minimal alluvial storage and suggest that most of the cosmogenic inventory of the samples is accumulated while eroding from bedrock and traveling down slope.**

**Cosmogenic results show that all the rivers that drain areas underlain by relatively unresistant lithologies, such as slates and siltstones, yield higher erosion rates than those that flow over sandstone or plutonic rocks. This result is also supported by cosmogenic nuclide analysis in bedrock outcrops which indicates the influence of lithology over erosion; more resistant lithologies erode slower than less resistant ones. Longitudinal profiles of the sampled streams indicate a correlation between knick point location and the outcropping of resistant lithologies, as well.**

**Grain size analysis in 6 alluvial sediment samples shows higher $^{10}Be$ activities in smaller grain sizes than in larger ones. The difference in activities arises from the large elevation distribution of the source of the smaller sedimentary particles compared with the narrow and relatively low elevation distribution of the large sedimentary particles and not from different generating rates. $^{26}Al/^{10}Be$ ratios do not show any indication of significant burial periods for our samples. However, alluvial samples show the lowest $^{26}Al/^{10}Be$, compared with bedrock and alluvium, an expected trend considering that sand size sediment spends the longest time ion the slopes and in the rivers.**

**The degree of correlation between $^{10}Be$ activities and erosion rates and several basin drainage physical parameters show that mean slope gradient influences basin-wide erosion rates the most and that alluvial parameters such as basin area and climatic factors are less significant. Being the first study to estimate sediment generation and erosion rates on a mountain range scale, our results confirm the established knowledge concerning the erosional history of the Appalachians since the rifting of the Atlantic Ocean. Our results confirm some of the basic ideas embedded in the *geographic cycle* model of Davis and the *dynamic equilibrium* model of Hack. Comparing our results with other measured and calculated erosion rates in the Appalachians, we conclude that relatively constant erosion has prevailed for hundreds of millions of years resulting in a steady state landscape.**

## INTRODUCTION

The Appalachian Mountains (fig. 1), one of the largest and most studied ancient orogenic belts, were built by a series of collisional events in the Paleozoic and an extensional event in the Late Triassic related to the opening of the Atlantic Ocean (Blackmer et al., 1994; Boettcher and Milliken, 1994; Friedman and Sanders, 1982; Pazzaglia and Brandon, 1996). Because the mountains are well studied and easily accessible, they provide an ideal setting to study post-orogenic processes particularly, the relationship between isostatically driven uplift and surface processes in old mountain belts.

The longevity of the Appalachians Mountains is striking. To understand the survival of these mountains, one needs to quantify the rate at which they erode over time and space. As a rapidly maturing field, cosmogenic nuclide analysis has proven to be a useful new tool for understanding rates of surface change. Cosmogenic isotopes are used to estimate rates of erosion at discreet locations on the landscape (e.g., Bierman and Turner, 1995; Small et al., 1999), rates of sediment production from individual drainages (e.g. Brown et al., 1995; Granger at al., 1996; Small et al., 1999; Clapp et al., 2000, Schaller et al., 2001), and rates of soil production (Heimsath, et al., 2001). The penetration depth of cosmic rays buffers the impact of both human-induced and naturally forced episodic erosion over several tens to hundreds of thousand of years (Bierman and Steig, 1996).

The Great Smoky Mountains (fig. 1), a well-studied range in the southern Appalachian Mountains, provide a natural setting to investigate the post-orogenic erosion processes that have been continuously active for more than 200 My. We measured cosmogenic $^{10}$Be and $^{26}$Al in bedrock, colluvium, and fluvial sediments to better understand the spatial pattern and rate of erosion in the Great Smoky Mountains. Analysis of cosmogenic nuclides in sediments has been tested previously in drainage basins of different sizes in different climates (Brown et al., 1995; Granger et al., 1996; Bierman and Steig, 1996; Clapp et al., 2000, 2001; Schaller et al., 2001; Bierman et al., 2001). This study represents the first significant application of cosmogenic nuclide analysis to the drainage basins of an old mountain range in a humid region.

## BACKGROUND

### *The Great Smoky Mountains*

The Great Smoky Mountains, located on the border between North Carolina and Tennessee, are the highest range in the southern Appalachian Mountains. They rise more than 1500 meters above the adjacent Little Tennessee River and French Broad River valleys. Relief in the Great Smoky Mountains is significant. Steep slopes connect flat ridge crests with deeply incised rivers (fig. 2). Slopes and mountain crests are soil covered and heavily vegetated (fig. 2). Mean annual rainfall ranges from 165 to 250 cm, depending on elevation (http://www.nps.gov/grsm/gsmsite/natureinfo.html; 11/01). Only minor gullying and storm-

related landslide scars are evident on hill slopes. Diffusive processes including tree throw (fig. 2), appear to control down slope movement of colluvium and soil.

The Great Smoky Mountains are built of medium grade, metamorphosed sedimentary rocks of Neoproterozoic to early Cambrian age with isolated areas of Mesoproterozoic gneiss (King et al., 1968). These rocks were transported perhaps 100 km westward to their current location above the Great Smoky thrust fault about 280 million years ago during the continental collision of the Alleghanian orogeny (King et al., 1968). The geology of the Great Smoky Mountains area has been studied for over 100 years (Keith, 1895; Glenn, 1926; Hadley and Goldsmith, 1963; King, 1964; Hamilton, 1961; **Southworth, 1995; 2000; Schultz, 1999; Schultz et al., 2000; Schultz and Southworth, 2000; Southworth, 2001**; Naeser et al., 1999; 2001). Although the constructional history, structure, and lithology of the range are fairly well understood, the spatial and temporal patterns by which the Appalachians have and are being eroded is not as well understood despite the long list of geomorphic studies, the first of which was completed over 100 years ago (Davis, 1899; Hack, 1960; 1979; Mills et al., 1987).

### *Physiography*

Our study area is within the Great Smoky Mountains National Park (fig. 1). Topographically, the Great Smoky Mountains are an island upland incised on three sides by valleys carved by the Little Tennessee River and Tuckasegee River to the south and west, and the Pigeon River to the east. The headwaters of these rivers originate southeast of the Great Smoky Mountains, and they flow to join the Ohio and Mississippi Rivers into the Gulf of Mexico. North of the Great Smoky Mountains, limestone and dolomite chemically weather to form the lowland of the Tennessee Valley, in stark physiographic contrast to the Great Smoky Mountains.

Four main river systems drain Great Smoky Mountains National Park (fig. 1): 1) the western tributaries of the Pigeon River, 2) the northern tributaries of the Tuckasegee River and Little Tennessee River, 3) the Little Pigeon River and, 4) the Little River. The Pigeon River-Little Tennessee/Tuckasegee River divide trends northerly along the Balsam Mountains and transects the strike of the regional geology. The drainage divide between the Little Tennessee-Tuckasegee Rivers and Little Pigeon River-Little River runs along the summit of the Great Smoky Mountains and follows the northeast strike of the regional geology. Within each of these main drainage systems, bedrock out crops, colluvium, and alluvial sediment were sampled for this study.

### *Structural and bedrock control of drainage systems*

Most drainages in the Great Smoky Mountains flow on bedrock but only a few appear to be controlled by bedrock structure. Parts of Abrams Creek, Twenty-Mile Creek, Eagle Creek, Hazel Creek, Forney Creek, Raven Fork, and Straight Fork flow parallel to the strike of

bedding and penetrative foliation in folded rocks (fig. 3). Only parts of the Oconaluftee River and Straight Fork flow parallel to interpreted and known faults such as the Oconaluftee Fault (fig. 3). Neotectonic activity is not supported by field evidence. However, post-Cretaceous motion, for example on the Gatlinburg Fault has been proposed on the basis of thermochronologic studies (Naeser et al., 2001).

The development of river terraces and the resultant storage of sediment appear to be greatly influenced by rock type and is mainly restricted to the perimeters of the mountain range. Terraces are found along the Tuckasegee River south of the Great Smoky Mountains and along the Raven Fork and Oconaluftee River in the Cherokee area of North Carolina, where the bedrock is granitic gneiss. Elsewhere, well-developed terraces are found where drainages cross carbonate rock and fine-grained metasiltstone. There are only few sites of significant alluvial storage with in the park's boundaries; thus, our interpretation of analysis is unaffected by long-term large-scale sediment storage. Most alluvial storage is located on the boundaries and outside of the Great Smoky Mountains National Park.

*Bedrock and morphology*

The Great Smoky Mountains are mostly underlain by resistant, quartz-rich, metamorphosed conglomeratic sandstone (Thunderhead Sandstone) and slate (Anakeesta Formation) of the Great Smoky Group (King, 1964, fig. 3). The Great Smoky Mountain drainage divide is subparallel to the strike of the metasandstone units. In the eastern part of the Great Smoky Mountains, the northwest side of the divide is characterized by the outcrop of massive southeast-dipping beds that form cliffs. These massive beds of metasandstone taper to the southwest where the cliffs and outcrop diminish. The distribution of large, inactive fan deposits such as the Cosby Fan in the northeast part of the park (fig. 3), which consist of coarse boulders of metasandstone, corresponds with the north-facing homoclinal outcrop slope of massive metasandstone cliffs. These boulder deposits show no evidence of historical activity other than incision. The southeast side of most of the divide is either a dip slope or folded units with poor outcrop. The Anakeesta Formation underlies a broad area of the divide in the eastern part of Great Smoky Mountains (fig. 3). This area is characterized by craggy topography with cliffs due in part to historical storm-related debris flows (**Schultz and others, 2000**). Mesoproterozoic granitic gneiss is exposed in antiforms in the south-southeastern part of Great Smoky Mountains.

Erosion of tectonic structures has created karst valleys. Extending across the base of the Great Smoky Mountains are karst valleys of Ordovician limestone preserved in the tectonic windows of the Great Smoky thrust fault (fig 3). Some of these valleys such as Cades Cove, Tuckaleechee Cove, and Wear Cove preserve fluvial terrace deposits and fan deposits of colluvium derived from the clastic rocks above the thrust fault high on the slopes.

*Surface processes*

Our field observations suggest the pattern and process by which mass is removed from the Great Smoky Mountains. Bedrock outcrops on slopes and on ridge tops are rare and mainly appear where the Thunderhead Formation sandstone is exposed. Infrequent outcrops suggest a balance between subsurface weathering rate of bedrock and down slope soil transport. This balance enables the development of soil practically throughout the entire slope environment, from stream channels to ridge crests. Scree slopes and coarse colluvial aprons on slopes are also not abundant. However, where they do exist, they originate in the Thunderhead Formation. Boulder deposits are generally located in the north side of the main water divide where the relationship between the regional strike and the north facing slopes enable the formation of cliffs. The age the coarse colluvial deposits is unknown **(any estimates for their age? If they are old, then their preservation is another indication of stability).** Recent mass wasting activity occurs mainly within the Anakeesta Formation slates (fig. 3) and is limited to small areas throughout the park.

The slopes and ridge crests are soil covered and heavily vegetated (fig. 2). Soil sections exhibit well-established horizons and consistent thickness suggesting their stability (A. Khiel, personal communication). The effect of raindrop impact is virtually negated by the dense canopy cover. The high organic matter content of the surface soils allows water to infiltrate very quickly, thus limiting overland flow, even during very high intensity rainfall. Most water flows along the soil-rock interface. There is very little evidence of soil stripping in the form of gullies and rills. Soil disturbance is mainly due to animal borrowing and tree throw. Fallen trees expose colluvial sections 1to 4 meters thick. Within the mountain range, storage of sediment appears restricted to the slopes. We did not observe significant river terraces or fans. The water in the rivers is generally clear. Even during high discharge events, the water remained clear not carrying much suspended load.

We sampled coarse colluvium at the lower part of a slope in the Raven Fork basin. Colluvial material was mostly fine grained and coarse clasts were nearly absent. In contrast, colluvium collected in sample GSC-4, only 70 meters below the outcrop of sample GSC-3, contained many coarse fragments. The difference in coarse material content in the colluvium suggests that coarse material occurs only in the proximity of its bedrock source and that it rapidly disintegrates into fine sand size as it moves down slope.

Overall, field observations indicate that sediment is generated by the alteration of rock to soil. Soil is transported steadily and slowly down slope by diffusive processes. Once the fine grain sediment reaches the stream, it is rapidly transported out of the mountain range. The field observation suggest the dominance of slope processes in the Great Smoky Mountains and implies that most of the cosmogenic nuclides we measured in the fluvial sediments accumulated while the material was on the hill slopes rather than in the stream system.

## METHODS

### *Sample collection*

To understand the pattern of erosion throughout the Great Smoky Mountains, we collected several types of samples (table 1, fig. 4): bedrock (n=10), colluvium (n=3), and fluvial sediments (n=43). These samples, including grain size splits of some sediment samples, were analyzed to determine the activity of $^{26}Al$ and $^{10}Be$.

*Exposed bedrock*.-The analysis of cosmogenic $^{26}Al$ and $^{10}Be$ activities in bedrock outcrops provides bedrock lowering rates at specific locations in the present topography. Since most of the ridge tops in the Great Smoky Mountains are soil covered, bedrock outcrops are rare. Samples were collected from outcrops on the main Great Smoky Mountains drainage divide and along the Cataloochee River-Raven Fork divide (fig. 4). All samples were taken on or within several meters of the local divides except for sample GSC-3, which was collected from an outcrop on a slope about 70 meters below the ridge top in the Raven Fork drainage basin. Most bedrock samples were collected from metamorphosed sandstone outcrops. Sample GSDV-6 was collected from a large quartz pegmatite. The pegmatite did not stand up above the adjacent sandstone. Sample GSC-3 was collected from a gneiss outcrop. Bedrock outcrops are 1 to 4 meters higher than the soiled-covered surface around them. Samples were taken from the upper flat surface of the outcrops. Sample thickness was ≤5 cm. There is no field evidence for exfoliation of the outcrops and they seem to erode in a continuous grain by grain process. Bedrock samples were crushed and the 0.25 to 0.85 mm fraction was purified to provide quartz for cosmogenic $^{26}Al$ and $^{10}Be$ analysis.

*Colluvium*.-Colluvium samples were collected in order to examine the residence time of relatively coarse material on the slope. Samples GSDV-5 and GSDV-9 are ridge top samples (fig. 4). They were collected, respectively, from around the outcrops where ridge top samples GSDV-4 and GSDV-8 were collected. Samples GSDV-5 and GSDV-9 were separated into 0.25 to 2 and >2 mm fractions to test whether nuclide activity vary with grain size. Sample GSC-4 was collected along contour ~70 meters below sample GSC-3. It is a slope sample (fig. 4) consisting of several hundreds of rock fragments (1 to 2 cm in diameter) that were mixed in a single sample. Pure quartz fragments were avoided. All fragments were crushed and the 0.25 to 0.85 mm fraction was purified for analysis

*Alluvium*.-Alluvial sediment were sampled from most of the outlet rivers (n=16, fig. 4) in the Great Smoky Mountains. Together, these basins drain 80% of the range's area. Our sampling strategy was designed to facilitate estimation of basin scale erosion rates, detect down stream trends in cosmogenic nuclide activity, and test basin scale parameters that might control erosion rates such as lithology, aspect, climate, and topographic location of samples. Sample GSCO-1 was taken below the confluence of the Raven Fork and the Oconaluftee River to test sediment mixing. Sample GSCO-1A is a replicate of GSCO-1; it was collected from the same location 4 months after sample GSCO-1 was collected. Sample GSBC-2 was taken as a

replicate of sample GSBC-1. Both were collected on the same day and they are about 1 km apart from each other. Sample GSCS-2 was taken from a small channel that drains only the Cosby Fan to estimate the nuclide activity of sediment that was originally transported in large mass wasting events **(scott-REF**).

Within three basins we sampled major tributaries in detail (Oconaluftee River, n=5; Raven Fork, n=11; Little River, n=6, fig. 5) to test the assumptions of thorough sediment mixing, minor alluvial storage, and to locate sediment sources. All the alluvial sediment samples were sampled from within river channels or from sandbars (fig. 2). Sand was collected and mixed from several locations across the channel. Sediment was sieved and the 0.25 to 0.85 mm fraction was analyzed for cosmogenic $^{26}$Al and $^{10}$Be in every sample. Six samples were separated to size fractions (0.25 to 0.85, 0.85 to 2, 2 to 10, >10 mm) to test whether different size grains have different cosmogenic nuclide activities, and relate differences to erosional processes (Brown et al., 1995).

### *Isotopic analysis*

All our samples were processed according to the approach detailed in Bierman and Caffee (2001). Cosmogenic $^{26}$Al and $^{10}$Be were measured at the Center for Accelerator Mass Spectrometry (AMS) at Livermore National Laboratory. Isotope ratio measurements were reduced to nuclide abundances using spread-sheet-based data reduction programs.

In order to interpret the nuclide data for alluvial sediments, basin-integrated nuclide production rates were estimated. The hypsometry of each basin was divided into 100 meter elevation bins and the effective cosmogenic nuclide production rate was calculated at the mid-elevation of each bin (Bierman and Steig, 1996; Brown et al., 1995; Granger et al., 1996). For large basins (>50 km$^2$), we determined basin hypsometery and calculated effective or integrated nuclide production rates using Digital Elevation Models (DEM). For small basins, we digitized 1:100000 topographic maps. We normalized our measured cosmogenic nuclide activities to sea level high latitude values using altitude/latitude/production relationships of Lal (1991) considering no muon production (Brown et al., 1995). We used a sea-level, high-latitude $^{10}$Be production rate of 5.17 atoms g$^{-1}$ yr$^{-1}$ supported by data from Bierman et al. (1996), Stone (2000), and Gosse and Stone (2001). The analytic precision of the measured samples considering AMS and stable nuclide concentrations is 3-5% (1$\sigma$). We propagate 10% uncertainty in production rates when making erosion rates and exposure age calculations. We did not specifically correct for variations in earth's magnetic field, topographic shielding, and muon production in depth.

### *Morphometry*

River profiles were digitized from 1:24000 maps. Geological and structural data (Hadley and Goldsmith, 1963; King, 1964; Hamilton, 1961; King et al., 1968) were added to

the profiles to test the relation between longitudinal profiles, bedrock, and structure. GIS procedures were used to derive physical parameters for each basin including: mean elevation, maximum elevation, relief ratio (ratio between the relief and distance between the highest and lowest points of the trunk channel), maximum relief (the elevation difference between the highest point in the basin and the sampling point), drainage basin area, mean slope gradient, and drainage density (km of channel per $km^2$ of basin area). These various parameters were correlated with model rates of erosion and $^{10}Be$ activities to assess their influence on the spatial pattern of erosion in the Great Smoky Mountains.

In the GIS analysis, a digital elevation model (DEM) of the Great Smoky Mountain region (USGS) was used as the base layer from which streams, watersheds, slope, and hypsometric curves were developed. The raster resolution of the DEM is 30 X 30 meter grid cells. Using ArcView in combination with a program extension named Prepro 0.3, the DEM was used to create a stream network as well as a watershed coverage. The Prepro program contains steps for modifying the DEM by filling sinks, computing flow direction, computing flow accumulation, and delineating stream networks. Delineating the stream networks requires specifying a threshold of DEM grid cells that defines the beginning of a stream. An acceptable threshold for stream definition of 75 cells (67500 $m^2$) was used to create a stream network from the DEM. Using the delineated stream network and the location of samples, the watersheds were delineated from the DEM. In each basin, elevation was divided into 100 meter bins (e.g. 100-200, 200-300, etc..) and the number of cells in each bin was counted and the area of each bin was calculated relatively to the total area of the basin.

Slope gradient distribution was calculated within each sampled basin. The slope gradient was derived from the DEM using ArcView and an extension called Spatial Analyst. The slope is derived by determining the maximum rate of elevation change between a grid cell and its neighbors within the DEM. This rate of change is given in degrees between 0 and 90. Drainage density was determined by the ratio between the total length of streams within each basin and the basin's area.

## DATA AND INTERPRETATION

### *Cosmogenic results*

*Bedrock samples*. - Bedrock samples collected from the Great Smoky Mountain (n=10) yielded measured $^{10}Be$ activities between $0.216\pm0.007 \times 10^6$ and $2.169\pm0.066 \times 10^6$ atoms $g^{-1}$ quartz and measured $^{26}Al$ activities between $0.000\pm0.000 \times 10^6$ and $0.000\pm0.000 \times 10^6$ atoms $g^{-1}$ quartz (table 2). A relation between the normalized $^{10}Be$ and $^{26}Al$ activities and bedrock lithology is apparent. The highest normalized $^{10}Be$ activity is from a quartz pegmatite sample (GSDV-6, $0.635\pm0.019 \times 10^6$ atoms $g^{-1}$ quartz). Lower normalized $^{10}Be$ activity was measured in a sample taken from basement gneiss (GSC-3, $0.197\pm0.005 \times 10^6$ atoms $g^{-1}$ quartz). All other

bedrock samples (n=8) were taken from sandstone of various formations and yield an average normalized $^{10}$Be activity of 0.101±0.031x10$^{6}$ atoms g$^{-1}$ quartz.

*Colluvium samples* - Colluvium samples (n=3) yielded measured $^{10}$Be activities between 0.173±0.012 x10$^{6}$ and 0.755±0.023 x10$^{6}$ atoms g$^{-1}$ quartz and measured $^{26}$Al activities between 1.069±0.069 x10$^{6}$ and 0.000±0.000 x10$^{6}$ atoms g$^{-1}$ quartz (table 2). The different grain fractions from samples GSDV-5 and GSDV-9 yielded similar $^{10}$Be and $^{26}$Al activities (table 2). This similarity implies that all grain fractions have similar dosing histories.

$^{10}$Be activities in the colluvium samples and their relation to adjacent bedrock outcrops can offer a spatial and temporal framework for the formation and movement of colluvium. Sample GSC-4, which was sampled ~70 meters below outcrop sample GSC-3 (0.470±0.015x10$^{6}$ atoms g$^{-1}$ quartz), yielded lower $^{10}$Be activity (0.173±0.012x10$^{6}$ atoms g$^{-1}$ quartz) than the outcrop (fig. 6). A similar pattern is presented by sample GSDV-9. Both grain sizes (0.25 to 2 and >2 mm) of this sample yielded similar $^{10}$Be activities of 0.333±0.011x10$^{6}$ and 0.305±0.010x10$^{6}$ atoms g$^{-1}$ quartz. This sample was collected from around the outcrop of sample GSDV-8 (0.346±0.013x10$^{6}$ atoms g$^{-1}$ quartz). This pattern is not always the case. Sample GSDV-5, that was collected around the outcrop of sample GSDV-4 ($^{10}$Be activity of 0.371±0.018x10$^{6}$ atoms g$^{-1}$ quartz) yielded higher than outcrop $^{10}$Be activities of 0.726±0.020x10$^{6}$ and 0.755±0.023x10$^{6}$ atoms g$^{-1}$ quartz for the 0.25 to 2 and the >2 mm fractions, respectively.

*Sediment samples*. - Sediment samples collected from the Great Smoky Mountain drainage systems (n=43) yielded measured $^{10}$Be activities between 0.178±0.006x10$^{6}$ and 0.461±0.012x10$^{6}$ atoms g$^{-1}$ quartz and measured $^{26}$Al activities between 0.000±0.000x10$^{6}$ and 0.000±0.000x10$^{6}$ atoms g$^{-1}$ quartz (table 3). Normalized $^{10}$Be activities in headwater tributary basins of the Raven Fork, Little River, and Oconaluftee River (for which there are no upstream samples; n=18) range between 0.184±0.005x10$^{6}$ and 0.064±0.002x10$^{6}$ atoms g$^{-1}$ quartz (table 3) with an average of 0.120±0.028 atoms g$^{-1}$ quartz. Normalized $^{10}$Be activities inferred from analysis of sediments collected from the outlet rivers (excluding Abrams Creek which drains large alluvial deposits from Cades Cove; n=15) that transport most of the sediment from the Great Smoky Mountains range between 0.093±0.003x10$^{6}$ and 0.174±0.007x10$^{6}$ atoms g$^{-1}$ quartz with an average of 0.139±0.029 atoms g$^{-1}$ quartz. The largest river (basin area, 330 km$^{2}$) draining the Great Smoky Mountains has a normalized $^{10}$Be activity of 0.119±0.004x10$^{6}$ atoms g$^{-1}$ quartz (the average of 0.25 to 0.85 mm grain fraction of samples GSCO-1 and GSCO-1A; table 3) similar to that of the headwater tributaries and the outlet rivers.

Two samples, GSAC-1 from Abrams Creek and GSCS-2 from the Cosby Fan, that were collected from locations that have significant sediment storage allow to test for the effect of storage on cosmogenic nuclide activities. These samples yielded the highest $^{10}$Be activities and lowest erosion rates, among all collected sediment samples. The Cosby Fan is one of the

largest boulder deposits in the Great Smoky Mountains (figs. 2 and 3). Two sediment samples were taken from the Cosby Fan. GSCS-1 is from the main channel that originates at the main water divide and dissects the fan. GSCS-2 was taken from a small stream that drains only the fan. Sample GSCS-1 yielded a $^{10}$Be activity of 0.191±0.005 x$10^6$ atoms $g^{-1}$ quartz. Sample GSCS-2 yielded a $^{10}$Be activity of 0.333±0.009 x$10^6$ atoms $g^{-1}$ quartz. This two-fold difference (which increases when normalized $^{10}$Be activities of the two samples are considered; table 3), probably arises from the residence time of material deposited in the boulder fan and has been exposed and eroding since then. The low erosion rate of the fan material and its slightly disturbed surface serve as an indicator of the relative stability of the Great Smoky Mountains.

Sample GSAC-1 yielded a $^{10}$Be activity of 0.362±0.001x$10^6$ atoms $g^{-1}$ quartz and a calculated erosion rate of 14 m $My^{-1}$, the lowest of all the samples in the sediment samples in the Great Smoky Mountains. Abrams Creek passes through Cades Cove, one of the few locations within the Great Smoky Mountains that stores significant alluvial sediment (fig. 3). It is, therefore, possible that the high $^{10}$Be activity in sample GSAC-1 reflects the residence time of the sediment in the cove. Samples GSAC-1 and GSCS-2 yielded high $^{10}$Be activities, as would be expected when alluvial storage and therefore, long dosing histories, occur within the drainage system.

*$^{26}$Al to $^{10}$Be ratios* - Since $^{26}$Al and $^{10}$Be are produced at a ratio of ~6 (Nishiizumi et al., 1989) but decay at different rates, their measured ratio can be used to detect burial periods during and after exposure (Lal and Arnold, 1985; Bierman et al., 1999; Bierman and Caffee, 2001; Granger et al., 2001). The average $^{26}$Al/$^{10}$Be in our samples is 5.8±0.5 (1σ), indicating no significant burial. Alluvial samples have a $^{26}$Al/$^{10}$Be of 5.7±0.4 (or 5.6±0.4 when larger than 0.25-0.85 mm grain fractions are not included). Colluvial samples have a $^{26}$Al/$^{10}$Be of 6.5±0.4. Bedrock samples have $^{26}$Al/$^{10}$Be of 6.1±0.4. It is apparent that none of the sample groups, bedrock, colluvium, or alluvium, experienced significant burial. However, the differences between the three groups, although subtle, might be real and arise from the process that transports mass in the Great Smoky Mountains. Alluvial samples, which have the longest dosing history of cosmic radiation, are expected to experience more events of burial on the slopes and in the stream system and therefore, yield the lowest $^{26}$Al/$^{10}$Be. The dosing history of bedrock outcrops is probably shorter and relatively simple. Thus, the $^{26}$Al/$^{10}$Be is higher and closer to 6. The process by which colluvium is produced and transported down slope is very complex and further investigation is needed to explain the $^{26}$Al/$^{10}$Be in colluvium.

*Grain size test*. – Grain size tests were carried out on 6 samples (table 4). In five samples, grain size tests indicate the influence of grain size on cosmogenic nuclide activity; smaller grain sizes yielded higher $^{10}$Be activities than larger grain sizes (fig. 7). The sixth sample, GSCO-7, which was collected from the headwaters of the Oconaluftee River yielded

similar measured $^{10}$Be activities in all grain size fractions ($0.278\pm0.007\times10^6$ to $0.305\pm0.008\times10^6$ atoms $g^{-1}$ quartz).

Samples GSCO-1 and GSCO-1A were collected from the same site, 4 months apart. $^{10}$Be activities in the small grain sizes (0.25 to 0.85, 0.85 to 2) from samples GSCO-1 ($0.264\pm0.01$, $0.266\pm0.007\times10^6$ atoms $g^{-1}$ quartz) and GSCO-1A ($0.295\pm0.009\times10^6$ and $0.292\pm0.010\times10^6$ atoms $g^{-1}$ quartz) exhibit a difference of only ~10%. This difference probably represents the natural cosmogenic nuclide variance within the sediments. $^{10}$Be activity from the >2 mm fraction of sample GSCO-1 is low ($0.165\pm0.004\times10^6$ atoms $g^{-1}$ quartz). The 2 to 10 mm fraction of sample GSCO-1A yielded a higher $^{10}$Be activity of $0.262\pm0.009\times10^6$ atoms $g^{-1}$ quartz. However, the largest (>10 mm) fraction of sample GSCO-1A yielded a $^{10}$Be activity of $0.189\pm0.006\times10^6$ atoms $g^{-1}$ quartz, similar to that of the >2 mm fraction of sample GSCO-1. This similarity suggests that most of the grains in sample GSCO-1 (>2 mm) probably were larger than 10 mm, and that they dominated the measured $^{10}$Be activity of the sample.

Three samples from the Little River also show that measured $^{10}$Be activity depends on grain size (table 4). As with the Oconaluftee River samples, the smaller grain fractions of the Little River samples yielded $^{10}$Be activities similar to those of the 0.25 to 0.85 and 0.85 to 2 mm fractions from the other rivers. However, the larger grain fractions (2 to 10 and >10 mm) yielded $^{10}$Be activities that range between $0.132\pm0.004\times10^6$ and $0.165\pm0.005\times10^6$ atoms $g^{-1}$ quartz (figure 7).

The smaller grain fractions (0.25 to 0.85 and 0.85 to 2 mm) from all the grain size test samples, yielded an average measured $^{10}$Be activity of $0.252\pm0.035\times10^6$ atoms $g^{-1}$ quartz and an average normalized $^{10}$Be activity of $0.100\pm0.019\times10^6$ atoms $g^{-1}$ quartz. This normalized activity is similar to that of the entire suit of alluvial sediments, suggesting that the fine sand grain size represent well the cosmic ray dosing history of the sediment transported out of the Great Smoky Mountains. The larger grain sizes (2 to 10, >10 and >2 in samples GSCO-1 and GSCO-7) yielded a large range of measured $^{10}$Be activities ($0.132\pm0.004\times10^6$ to $0.305\pm0.008\times10^6$ atoms $g^{-1}$ quartz) with an average of $0.182\pm0.057\times10^6$ atoms $g^{-1}$ quartz. When sample GSCO-7 (the sample that showed no grain size effect) is excluded, the average measured $^{10}$Be activity of the larger grain sizes decreases to $0.168\pm0.039\times10^6$, lower than that of the smaller grain sizes.

### *Morphometry*

The longitudinal profiles of the sampled outlet rivers indicate that in most cases, river channels are graded and approach a steady state profile (Whipple, 2001; fig. 8). Most rivers are concave upwards with a steep reach at the headwaters. Within several km from the divide the stream gradient decreases. However, there are several exceptions. Major knick-points and convex upwards reaches appear in several of the profiles. The most prominent is the one in Raven Fork. Similar reaches appear also in the profiles of Bunches Creek, Eagle Creek, the

Little Pigeon River, the Middle Prong of the Little River, and the West prong of the Little Pigeon River (fig. 8).

In the Middle Prong of the Little River, the Little Pigeon River (cross section from Mt. Kephat), and the West Prong of the Little Pigeon River there is a relation between the convex upward reaches and the underlying Thunderhead Formation sandstone, especially where it out crops adjacent to the less resistant slates of the Anakeesta Formation, suggesting a lithologic control on the stream profile. In Eagle Creek, Little Pigeon River (cross section from Tri-Corner), Bunches Creek, and Twenty Mile Creek there is no apparent lithological explanation for the change in gradient of the stream and for the development of a knick-point. Intraformational variations of the resistance of sandstone to erosion might serve as a possible explanation. The major knick-point in the Raven Fork is associated with the outcropping of the Grenville Basement. Knick-points associated with faults are not seen in the longitudinal profiles, suggesting no recent activity of the faults crossed by the streams. The topographic profile of Parsons Branch is also anomalous. It does not display the upper steep reach and the lower gentle reach. The profile of Parsons Branch suggests that it may have been beheaded and that it was once part of an antecedent route of a larger river.

The normalized $^{10}$Be activities plotted against physical parameters of the different sampled basin (fig. 9) indicate low correlation with basin maximum elevation ($r^2$=0.12) and average elevation ($r^2$=0.22). There is no correlation between $^{10}$Be activities and basin relief, relief ratio, the distance from the western end of park, drainage density, and drainage area. A higher correlation ($r^2$=0.42) exists between $^{10}$Be activities and basin mean slope gradient.

## DISCUSSION

Several studies have applied $^{10}$Be and $^{26}$Al activities in sediments to understand various aspects of landscape development. Bierman and Steig (1996) and Granger at al., (1996) tested the applicability of sampling cosmogenic nuclide concentrations in alluvial sediments to estimate basin-wide average erosion rates. Both showed that, pending on several assumptions, cosmogenic nuclide concentrations in alluvial sediments can be interpreted in terms of average sediment generation rates and basin-wide erosion rates. Brown et al., (1995) applied $^{10}$Be measurements in sediments from a small watershed in Puerto-Rico to distinguish sources of different grain sized sedimentary particles. They concluded that particles larger than 1 mm were contributed by mass wasting processes and those smaller than 1 mm were contributed by the continuous weathering of bedrock to soil. The cosmogenic nuclide concentration dependency on grain size was not detected by later studies in arid environments (Clapp et al., 2000; 2001; in press). A study by Schaller et al. (2001) in the temperate climate of Central Europe did not detect a dependency between grain size and cosmogenic nuclide activity, either. However, in their study, Schaller et al. (2001) reached several conclusion that support our conclusions in the present study. Mainly, that average erosion rates are similar to uplift rates in

this tectonically inactive region, hill slope processes are dominated by diffusive processes, grain size does not affect cosmogenic nuclide concentrations, and that lithology influences erosion rates.

The use of cosmogenic nuclide activity in alluvial sediments to estimate erosion rates enables the comparison between short-term and long-term sediment generation rates. Several studies compare short and long-term rates in order to present temporal variation and human influence on landscape development (Kirchner et al., 2001). Testing parameters that control erosion on a basin scale is also possible. Riebe et al. (2000; 2001) sampled alluvial sediments from small catchments in seven sites in the Sierra Nevada, and tested the relation between basin wide erosion rates with proximity to regions of rapid base level lowering and climate.

The present study is the first to investigate the temporal and spatial pattern of a complete mountain range. We applied cosmogenic nuclide concentrations in alluvial sediments together with measuring cosmogenic nuclide concentrations in bedrock and colluvial sediments and then integrated the results with other short and long-term estimates of erosion rates. The spatial distribution of our samples enabled the assessment of lithology, climate and topographic characteristics as factors controlling erosion rates. We were able to determine the roll of grain size on the cosmogenic nuclide concentrations and show that fine sand grain size represents the average dosing history of sediments in each sampled basin. Our results also enable the assessment of steady-state landscape and equilibrium between erosion and uplifting processes in the southern Appalachian Mountains, as will be discussed below.

*Validation of assumptions and Great Smoky Mountain erosion rates*

Cosmogenic nuclide activities in sediments indicate basin-wide average dosing history (Bierman and Steig, 1996). By assuming the following assumptions, dosing history can be reduced to sediment generation and erosion rates: (1) Rate of erosion is constant over the time sampled by cosmogenic isotopes; (2) Sediment storage within the sampled basin is constant or minimal; (3) The target mineral, (quartz) is homogeneously distributed with in the sampled basin (4) Sediment is well mixed. The first assumption is difficult to prove and we must accept the model erosion rates as average rates. Alluvial sediment storage in the mountain range is minimal as the river valleys lack large terraces, fans, and flood plains. Our data show no downstream increase in $^{10}$Be activities within the rivers that were sampled in detail, confirming the field observation of insignificant alluvial storage and suggesting that most measured $^{10}$Be is produced by cosmic-ray dosing on hill slopes rather than during fluvial transport. Although sediment is stored on the slopes, the stability of the soil mantle indicates constant storage. Most of the Great Smoky Mountains are underlain by quartz rich lithologies such as sandstone and gneiss (Hadley and Goldsmith, 1963; King, 1964; Hamilton, 1961). Thorough mixing of sediment from different tributaries can be tested by a mass balance calculation (ref – geology).

*Grain size test*.- The difference in cosmogenic nuclide activity of the various size grains is caused by differences in their average exposure history. Brown et al. (1995) showed that lower $^{10}$Be activities of larger size fractions can be explained by mass wasting events that carry coarse material rapidly down slope. However, there is no field evidence to indicate high or even significant frequency of mass wasting events, such as mud and rockslides in our study area. Therefore, it is more likely that the difference in activities between the smaller and larger grain fractions represents the average residence time of the different fractions on the slope and the elevation distribution from where they originate.

The mobility of larger clasts is much lower than that of sand (Ferguson et al., 1996; Ferguson and Wathen, 1998), therefore, it is reasonable to assume that most of the sampled clasts were derived from the adjacent slopes and that they were not transported for long distances down stream. Furthermore, not all clasts that reside on the slope actually reach the stream. Clasts from the upper parts of the slope are likely to disintegrate to sand before they reach the stream due to intense chemical weathering. This suggestion is supported by the field observations mentioned earlier. Only clasts that originate and are exposed at the lower part of the slope can reach the stream before completely disintegrating into the fine sand grain size **(REF for chemical erosion down slope)**. Thus, the sampled clasts are mostly derived from the lower parts of the adjacent slopes. This reduces both their total average exposure history and the effective $^{10}$Be production rate. Consequently they yield lower $^{10}$Be activities (fig. 7). This process does not occur in arid climates due to the low chemical weathering rate that allows clasts originating throughout the basin to reach the streams and then be transported during floods with the fine grain material. Thus, in arid climates, differences in $^{10}$Be activities among the different grain sizes are insignificant (Clapp et al., 2000; 2001; in press).

When $^{10}$Be activities are interpreted as erosion rates using the effective basin-wide production rate, larger grain sizes yield higher erosion rates than smaller grain sizes (table 5, fig. 7). However, since we assume that the larger clasts originate only from the lower part of the slopes adjacent to the sampling locations, the effective basin-wide production rate does not properly describe the $^{10}$Be production in them. The improper use of the basin-wide production rate for the larger grain sizes becomes more apparent with the increase in basin relief. Among the basins that were sampled for grain size effect, those with the greater elevation difference (and by inference a greater difference between the sampling site production rate and the effective basin-wide production rate), such as GSCO-1 (~1000 m; $\Delta P$=37%) and GSLR-7 (~1400 m; $\Delta P$=34%), showed a greater difference in normalized $^{10}$Be activities between the smaller and larger grain sizes. In the basin that has the smallest elevation difference (~300 m), and the smallest difference between sampling site production rate and the effective basin-wide production rate ($\Delta P$=14%), $^{10}$Be activities were similar in all grain size fractions (sample GSCO-7, fig. 7). This positive correlation between maximum relief in the basin and difference

in normalized $^{10}$Be activities suggests that the larger grain sizes originate from lower elevations than the smaller grain sizes.

To accurately calculate erosion rates from the measured $^{10}$Be activities in the larger clasts it is required to use a production rate that will describe the elevation distribution from which they originated. It is of course impossible to calculate the effective production rate for the larger clasts. However, it seems to us that the lower production rate of the sampling location, which is the lower elevation limit from where the clasts can originate, is a good proxy and will better describe the $^{10}$Be production within the clasts. When using these lower production rates, large grain fractions yield erosion rates similar to those calculated from the small grain fractions (fig. 7). This manipulation of the grain size test results indicates that there is no actual difference in process and rate at which different grain sizes erode in the Great Smoky Mountains. It also verify that the fine sand grain size that was analyzed in alluvial sediments throughout the Great Smoky Mountains and the erosion rates calculated from the $^{10}$Be activities in those samples represent the erosional processes and rates which occur in that mountain range.

*Bedrock*.-$^{10}$Be activities in bedrock samples are consistent with model erosion rates between 48.0±6.1 and 4.7±0.6 m My$^{-1}$ and $^{26}$Al activities with model erosion rates between 00.0±0.0 and 0.0±0.0 m My$^{-1}$ (fig. 4, table 6), with an average of 29.0±12.7 (1σ) m My$^{-1}$ **(paul – should the average be that of the Be and Al averages?)** (Lal, 1988)**.** Bedrock $^{10}$Be activities are consistent with sediment generation rates between 130±17 and 13±2 tons km$^{-2}$ yr$^{-1}$ with an average of 78±34 tons km$^{-2}$ yr$^{-1}$ (or 91±23 tons km$^{-2}$ yr$^{-1}$ for sandstone when gneiss and quartzite samples GSC-3 and GSDV-6 are excluded).

*Colluvium*.- The small population of colluvium samples does not indicate a consistent relationship between cosmogenic nuclide activities in colluvium and adjacent bedrock. It is possible that the random stirring of sediment through the thick soil column during down slope movement (Heimsath et al., 2002) results in a highly variable cosmogenic nuclide abundance in the different samples relative to exposed bedrock nuclide activity. Furthermore, exposed bedrock in the Great Smoky Mountains is rare, and most bedrock erosion is subsurface. A much larger and detailed sampled population is needed to reveal the relation between bedrock and colluvium dosing histories.

*Alluvium*.-Using the interpretive model of Bierman and Steig (1996), $^{10}$Be activities in our alluvial samples are consistent with sediment generation rates between 38 and 133 tons km$^{-2}$ yr$^{-1}$, the equivalent of model erosion rates between 14.0±1.8 and 49.1±6.3 m My$^{-1}$ (table 7, fig. 4). $^{26}$Al activities are consistent with sediment generation rates between 00 and 000 tons km$^{-2}$ yr$^{-1}$, the equivalent of model erosion rates between 00.0±0.0 and 00.0±0.0 m My$^{-1}$ (table 7). All the samples that yielded erosion rates higher than 30 m My$^{-1}$ were collected from rivers that cross through areas underlain by the Anakeesta Formation slats and/or the Pigeon

Formation siltstones. This correlation between high erosion rates and relatively erodable rock types points at the importance of lithology in determining erosion rates. Erosion rates in headwater tributary basins of the Raven Fork, Little River, and Oconaluftee River (for which there are no upstream samples; n=18) range from 16.9 to 49.1 m $My^{-1}$ (table 7, fig. 5) with an average of 27.6±7.4 $mMy^{-1}$. Basin scale erosion rates inferred from analysis of sediments collected from the outlet rivers (n=16) that transport most of the sediment from the Great Smoky Mountains range from 14.0 to 33.7 m $My^{-1}$ with an average of 23.2±5.9 m $My^{-1}$. However, when excluding sample GSAC-1, which passes through Cades Cove, which might store alluvial material, the outlet river average erosion rate is 24.3±5.6 m $My^{-1}$. The largest river (basin area, 330 $km^2$) draining the Great Smoky Mountains has a basin average erosion rate of 26.3±5.2 m $My^{-1}$ (the average of 0.25 to 0.85 mm grain fraction of samples GSCO-1 and GSCO-1A; table 7) similar to that of the headwater tributaries and the outlet rivers. The consistency of normalized $^{10}Be$ activities and average erosion rates with increasing basin area indicates the thorough mixing and the rapid movement of sediment in the alluvial channel and supports the observation of minimal alluvial sediment storage and suggests the uniform average erosion of all parts of the alluvial system.

The weighted-average sediment generation rate of the outlet rivers implied by cosmogenic nuclide concentration is 63±16 tons $km^{-2}$ $yr^{-1}$ (n=16). This rate is lower than that implied by bedrock erosion (91±23 tons $km^{-2}$, n=10). This difference between the two rates might indicate an imbalance between the rate of sediment production as interpreted from bedrock outcrop $^{10}Be$ activities and the rate of sediment export out of the mountain range and imply increasing storage within the drainage basin. It is proposed, however, that the imbalance is only apparent and results from the shielding history of the bedrock outcrops. Although bedrock samples were collected from the upper flat surfaces of the outcrops, it is likely, in this humid environment, that they were partially or totally shielded for various periods of time by soil, roots, and trees. Furthermore, the geometry of the outcrop might have changed during the time span that is averaged by the $^{10}Be$ analysis. The shielding was not sufficient to alter significantly the $^{26}Al/^{10}Be$ (which for bedrock is 6.1±0.4). However, it reduced the effective average production rate of cosmogenic nuclides within the outcrop. Therefore, the actual erosion and sediment generation rates inferred from $^{10}Be$ activities in bedrock are maximum rates and are probably lower and are more similar to those implied by $^{10}Be$ activities in fluvial sediments. This apparent imbalance becomes even less important when considering the fact that bedrock outcrops are rare and most sediment in the Great Smoky Mountains originates from the subsurface erosion of buried bedrock.

*Parameters controlling $^{10}$Be activities erosion rates*

The degree of correlation between $^{10}$Be activities, model rates of erosion and the various drainage basin physical parameters indicates that colluvial processes influence the spatial pattern of erosion in the Great Smoky Mountains, and that alluvial processes and precipitation are less significant. Slope parameters show medium to low correlation with erosion rates. However, alluvial parameters, such as basin area, relief ratio, and drainage density are not correlated with erosion rates (fig. 9). Model erosion rates are positively correlated to the mean slope gradient within each drainage system ($R^2$= 0.42, fig. 9). It is likely that the steeper the slopes, the stability of the soil decreases, tree throw events occur more often and sediment is transported down slope more rapidly. This scenario would shorten the residence time of the colluvium on steep slopes and would result in lower cosmogenic isotope activities and higher model erosion rates. The correlation, although weak, between rates of erosion and average elevation ($R^2$= 0.22) or maximum basin elevation ($R^2$= 0.12) might result from a weak orographic affect. The weak orographic affect is supported by the weak correlation between erosion rates and the source of precipitation. Most of the precipitation that falls on the Great Smoky Mountain is delivered by storms approaching from the northwest (**REF**). Rivers that flow north of the main water divide have a higher average rate of erosion (29.4±7.8 m My$^{-1}$) compared with the average rate of erosion of the rivers that flow south of the main drainage divide (22.9±4.8 m My$^{-1}$) suggesting a rain shadow affect. Nevertheless, the weak correlation between erosion rates and distance from the western end of the mountain range (fig. 9) supports the fact that climatic variations do not influence erosion rates in the Great Smoky Mountains.

Rates of erosion do not correlate with drainage basin area. However, mean erosion rates are similar whether calculated from headwater tributaries, or from outlet rivers. For example, the 4 largest basins have $^{10}$Be model erosion rates (24.0±6.2 m My$^{-1}$), similar to the mean erosion rate of all the outlet rivers (23.2±5.9 m My$^{-1}$ or 24.3±5.6 m My$^{-1}$ when sample GSAC-1 is not included) and of the 18 smaller headwater basins (27.6±7.4 m My$^{-1}$).

Various basin drainage physical parameters have been examined in earlier studies and are considered as important in controlling erosion rates. Summerfield and Hulton (1994) concluded that basin relief ratio is one of the most important factors controlling erosion rates where as drainage basin area is less significant. Hovius (1998) and Milliman and Syvitski (1992) showed the importance of basin area and maximum basin elevation in tectonically active mountain belts. However, Hovius (1998), Milliman and Syvitski (1992) and Pinet and souriau (1988) show that the importance of basin area decreases dramatically when ancient orogenies (such as the Appalachian Mountains) are considered. Ahnert (1970), in his well cited study, determined that mean basin relief is the most significant factor controlling erosion rates while precipitation was of much less importance. This result agrees with Schumm (1963) who

reached the same conclusion. All these studies were carried out on medium to large drainage basins (generally $>10^4$ km$^2$) and denudation rates were based on sediment load measurements.

In the present study, we show that basin wide erosion rates, averaged over $10^3$-$10^5$ years, using cosmogenic nuclide measurements, depend only on basin mean slope gradient, and that other factors such as basin area, maximum basin elevation, and precipitation are less significant. The difference between the results of the present study and previous studies might arise from the fact that previous studies considered drainage basin from various tectonic environments, by that attributing common controlling factors to regions which are topographically developing and eroding through different processes. Hovius (1998), Milliman and Syvitski (1992), and Pinet and Souriau (1988) recognized this problem, and separated the basins they analyzed according to the level of tectonic activity and showed that basins in different tectonic environments depend differently on physical factors. They showed that in tectonically inactive mountains, such as the Appalachian Mountains, the dependency of sediment yield (and by inference denudation rates) on basin area is very weak compared to high tectonically active mountain belts. Our study, which was conducted in a single tectonic environment, confirms this result, shows the dominant importance of slope gradient on the erosion pattern, and highlights the problems in interpreting erosion rate spatial patterns when basins from various tectonic environments are considered.

### *Steady State of Great Smoky Mountains*

Some basic concepts of geomorphology were developed in reference to the Appalachian Mountains. In the old landscape of this mountain range, where active tectonics ceased long ago and glaciation did not take hold, topography had time to adjust and approach steady state. The *geographic cycle* developed by Davis (1899) stemmed from his observations and ideas in the hills of Pennsylvania. Although the *geographic cycle*, as a unifying geomorphologic model, has been abandoned, it is interesting to note the applicability of some of its ideas to our results. The Davisian *geographic cycle* describes the change in average relief of the landscape in a way that the initial relief, after tectonic uplifting ended, increases (during the youth stage) to a maximum due to deep river incision. Relief then decreases as hill crests are lowered towards the graded rivers. This lowering implies that slope processes are the main mechanisms of erosion during the mature and old stages of the landscape cycle. This description agrees with our observations and results, indicating the major role of slope processes in the erosion of the Great Smoky Mountains.

The *geographic cycle* model of Davis did not stand the test of time, due to his disregard to the influence of lithology and structure over the developing landscape. The *dynamic equilibrium* concept, proposed by Hack (1960), was developed in the Appalachians, where the relationship between topography, lithology, and structure could be observed. *Dynamic equilibrium* lead to the development of a steady state landscape, where relief is constant and

"…all elements of topography are mutually adjusted so that they are down wasting at the same rate" (Hack, 1960). Cosmogenic results from and longitudinal profiles of our sampled streams, which reveal the relation between lithology and the location of knick points in the rivers, indicate the long lasting importance of lithology over the rates of erosion in the mountain range. In the Great Smoky Mountains, erosion stabilized at a rate of ~30 m $My^{-1}$, a rate which suited the climatic, structural, and lithologic setting of the mountain belt and that enabled equilibrium between isostatically driven uplift and denudation. At this average rate of erosion, about 6-7 km of rock would have been eroded from the mountain range since the Jurassic, ~180 Ma.

The understanding of the landscape development of the Atlantic passive margin and its present topography stems from a variety of studies that investigated the structure and stratigraphy of the coastal plain and off shore basins. The initial topography of the Appalachians following the Alleghenian orogeny might have been similar to that of Cenozoic mountain-belts with an average elevation of 3000-4000 m. (Slingerland and Furlong, 1989). Rapid erosion during the Permian and Triassic removed most of this mass (and topography) into west lying basins. An increase in topography and relief occurred during the Jurassic rifting and opening of the Atlantic Ocean (Judson, 1975). The eastern off shore basins that formed at that time contain sedimentary sequences of at least 7 km of detritus shed off the Appalachian Mountains since the onset of Atlantic rifting, ~180 Ma. (Poag and Sevon, 1989). The sedimentary sequence in the off shore basins indicates rapid accumulation during the Jurassic, following the initial stages of sea floor spreading in the Atlantic, several periods of rapid accumulation during the Cretaceous and a large pulse of ciliciclastic sediment flux during the Miocene (Pazzaglia and Gardner, 2000). The later period of increased sedimentary flux is supported by fission track dating (Roden and Miller, 1989; Boettcher and Milliken, 1994). Variations in accumulation rates in the off shore basins were attributed to increases and decreases in erosion rates in the Appalachian Mountains. However, the driving forces for erosion rate and sediment flux changes are not well constrained and are explained by different mechanisms ranging from tectonic (Hack, 1982) to climatic ones (Barron, 1989). Our study, which is the first in its scale, measures in an almost direct way sediment generation rates from a major mountain range over a $10^4$-$10^5$ year time span. The results of our study confirm quantitatively assessments of erosion rates through the late Cenozoic in the southern Appalachians. Our results, when extrapolated over the last 180 My, imply 6-7 km of unroofing, similar to the sedimentary volume measured in the Atlantic off shore basins. Rates of erosion calculated in this study are also consistent with fission track data that imply 1-1.5 km of unroofing in the last 20 My (Zimmerman, 1979).

The comparison between short-term erosion rates calculated from sediment yield measurements (Hack, 1979; Menard, 1961; Judson, 1968; Judson and Ritter, 1964; Gilluly, 1964; Gordon, 1979; http://webserver.cr.usgs.gov/sediment/plsql/stateanchor; 6/01), Cenozoic

and Mesozoic erosion rates calculated using fission track analysis (Naeser et al., 1999, 2001; Zimmerman, 1979; Doherty and Lyons, 1980) and sediment budgets (Menard, 1961), the emplacement depths of presently exposed igneous intrusions (Zen, 1991), and Paleozoic erosion rates (Huvler, 1996; Zen, 1991; Pavich, 1985; Sutter, et al., 1985) suggest that high rates of denudation (>100 m $My^{-1}$) which accompanied the orogenic process, decreased dramatically after the termination of tectonically driven uplift (**REF-geology**). The low rates of erosion have been maintained for almost 200 My enabling balance between erosion and rock uplift. Such temporal similarity implies that the Great Smoky Mountains may be a steady-state landscape, when considered on time scales longer than $10^5$ to $10^6$ (Pazzaglia and Brandon, 2001; Whipple, 2001), the result of Hack's dynamic equilibrium persisting over $10^7$ years on the spatial scale of a mountain range. The results of this study are in contrast to models that predict that initial elevation and relief are reduced by 90% in as little as 60 million years (Ahnert, 1970) or that complete erosion of a continent to sea level would occur within 100 to 300 My (Pinet and Souriau, 1988; Harrison, 1994) and suggest the longevity of mountain belts. Despite erosion at rates of about 30 m $My^{-1}$ for the last 180 My, the southern Appalachian Mountains have prominent topographic expression and significant relief.

## CONCLUSIONS

Cosmogenic results indicate the spatial homogeneity of erosion rates in the Great Smoky Mountains at a rate of 25-30 m $My^{-1}$. These results, which indicate thorough mixing of sediment from different sources, rapid transport of sediment through the alluvial system, and minor alluvial storage validate the assumptions on which calculations of sediment generation and erosion rates are based on. The similar erosion rates calculated from $^{10}Be$ activity in bedrock, alluvial sediments in headwater tributaries and outlet rivers suggest that the entire range is being lowered at a similar rate while relief is being maintained or decreases very slowly. Cosmogenic results, field observations, and analysis of parameters controlling erosion indicate the importance of slope processes in determining the spatial pattern of erosion in the Great Smoky Mountains. The data sets suggest that most of the cosmogenic nuclide accumulation occurs on the slopes and that the rate of slope processes control the erosion in the mountain range while alluvial and climatic factors are less significant. $^{10}Be$ activities in bedrock and alluvium and longitudinal profiles of the streams that were sampled indicate a lithologic control over erosion rates. This result agrees with one of Hack's (1960, 1979) basic observations and with similar results by Schaller et al., (2001) that measured $^{10}Be$ activities in Central Europe river systems. In contrast, the longitudinal profiles do not indicate neotectonic activity on any of the faults crossed by the sampled streams in the Great Smoky Mountains.

Grain size analysis in alluvial sediment samples shows higher activities in smaller grain sizes than in larger ones. The difference in activities arises from the large elevation distribution

of the source of the smaller sedimentary particles compared with the narrow and relatively low elevation distribution of the large sedimentary particles.

Our results agree with the overall understanding of the denudational history of the Appalachians since the rifting of the Atlantic Ocean. Extrapolating the average erosion rates we calculated in this study over the time span since the Atlantic rifting (~200 My) yields a total eroded section of 6-7 km of rock. This amount of eroded rock agrees well with the volume of deposited sediments in the off shore Atlantic sedimentary basins. The comparison of erosion rates, calculated by various methods, in the Great Smoky Mountains and the southern Appalachians show that high erosion rates prevailed during the Paleozoic orogenic events that formed the Appalachians. These rates decreased to an average and steady erosion rate of about 30 m $My^{-1}$. This erosion rate balanced the rate of isostatically driven uplift and enabled the development of a steady state landscape in the Great Smoky Mountains.

ACKNOWLEDGMENTS

USGS, NSF, Critical writing class,

REFERENCES

Ahnert, F., 1970, Functional relationships between denudation, relief, and uplift in large mid-latitude drainage basins: American Journal of Science, v. 268, p. 243-263.

Barron, E.J., 1989, Climate variation and the Appalachians from the late Paleozoic to the present: Results from model simulations: Geomorphology, v. 2, p. 99-118.

Bierman, P., and Turner, J., 1995, $^{10}$Be and $^{26}$Al evidence for exceptionally low rates of Australian bedrock erosion and the likely existence of pre-Pleistocene landscapes: Quaternary Research, v. 44, p. 378-382.

Bierman, P., Larsen, P., Clapp, E., and Clark, D., 1996, Refining estimates of $^{10}$Be and $^{26}$Al production rates: Radiocarbon, v. 38, no. 1, p. 149-173.

Bierman, P., and Steig, E., 1996, Estimating rates of denudation and sediment transport using cosmogenic isotope abundances in sediment: Earth Surface Processes and Landforms, v. 21, p. 125-139.

Bierman, P.R., Marsella, K.A., Davis, P.T., Patterson, C., and Caffee, M., 1999, Mid-Pleistocene cosmogenic minimum-age limits for pre-Wisconsinan glacial surfaces in southwestern Minnesota and southern Baffin Island -- a multiple nuclide approach: Geomorphology, v. 27, p. 25-40.

Bierman, P., Clapp, E.M., Nichols, K.K., Gillespie, A.R., and Caffee, M., 2001, Using cosmogenic nuclide measurements in sediments to understand background rates of erosion and sediment transport, in: Harmon R.S., and Doe W.W., (eds.), Landscape erosion and evolution, Kluer/Plenum, New York, p. 89-116.

Bierman, P. R., and Caffee, M., 2001, Steady state rates of rock surface erosion and sediment production across the hyperarid Namib desert and the Namibian escarpment, southern Africa: American Journal of Science, v. 301, p. 326-358.

Blackmer, G. C., Omar, G. I., and Gold, D. P., 1994, Post-Alleghanian unroofing history of the Appalachian basin, Pennsylvania, from fission track analysis and thermal models: Tectonics, v. 13, p. 1259-1276.

Boettcher, S. S. and Milliken, K. L., 1994, Mesozoic-Cenozoic unroofing of the southern Appalachian basin: apatite fission track evidence from Middle Pennsylvanian Sandstones: Journal of Geology, v. 102, p. 655-663.

Brown, E., Stallard, R.F., Larsen, M.C., Raisbeck, G.M., and Yiou, F., 1995, Denudation rates determined from the accumulation of in situ-produced $^{10}$Be in the Luquillo Experimental Forest, Puerto Rico: Earth and Planetary Science Letters, v. 129, p. 193-202.

Clapp, E., Bierman, P.R., Schick, A.P., Lekach, Y., Enzel, Y., and Caffee, M., 2000, Sediment yield exceeds sediment production in arid region drainage basins: Geology, v. 28, p. 995-998.

Clapp E., Bierman P.R., Nichols K.K., Pavich M., and Caffee M., 2001, Rates of sediment supply to arroyos from upland erosion determined using in situ produced cosmogenic $^{10}$Be and $^{26}$Al: Quaternary Research, v. 55, p. 235-245.

Clapp E., Bierman P.R., and Caffee M., in press, Using $^{10}$Be and $^{26}$Al to determine sediment generation rates and identify sediment source areas in an arid region drainage basin: Geomorphology.

Davis, W. M., 1899, The geographical cycle: Journal of Geography, v. 14, p. 481-504.

Doherty, J.T., and Lyons, J.B., 1980, Mesozoic erosion rates in northern New England: Geological Society of America Bulletin, v. 91, p. 16-20.

Ferguson, R.I., and Wathen, S.J., 1998, Tracer-pebble movement along a concave river profile: Virtual velocity in relation to grain size and shear stress: Water Resources Research, v. 34, no. 8, p. 2031-2038.

Ferguson, R.I., Hoey, T., Wathen, S.J., and Werritty, A., 1996, field evidence for rapid downstream fining of river gravels through selective transport: Geology, v. 24, no. 2, p. 179-182.

Friedman, G. M. and Sanders, J. E., 1982, Time-temperature-burial significance of Devonian anthracite implies former great (~6.5 km) depth of burial of Catskill Mountains, New York: Geology, v. 10, p. 93-96.

Gilluly, J., 1964, Atlantic sediments, erosion rates, and the evolution of the continental shelf: some speculation: Geological Society of America Bulletin, v. 75, p. 483-492.

Glenn, L. C., 1926, The geology of the proposed Great Smoky Mountains National park, Journal of the Tennessee Academy of Science 1, no. 2: 13-15. Publisher: Host Item: Tennessee Academy of Science, United States.

Gordon, R.B., 1979, Denudation rate of central New England determined from estuarine sedimentation: American Journal of Science, v. 279, p. 632-642.

Gosse, J.C., and Stone, J., 2001, Terrestrial cosmogenic nuclide methods passing milestones toward paleo-altimetry: Eos, Transactions, American Geophysical Union, v, 82, no. 7, p. 82, 86, 89.

Granger, D.E., and Muzikar, P.F., 2001, Dating sediment burial with in situ produced cosmogenic nuclides: theory, techniques, and limitations: Earth and Planetary Science Letters, v. 188, p. 269-281.

Granger, D.E., Kirchner, J.W., and Finkel, R., 1996, Spatially averaged long-term erosion rates measured from in-situ produced cosmogenic nuclides in alluvial sediment: Journal of Geology, v. 104, p. 249-257.

Hack, J.T., 1982, Physiographic divisions and differential uplift in the Piedmont and Blue ridge: U.S. Geological Survey Professional Paper 1265, 49 pp.

Hack, J.T., 1979, Rock control and tectonism, their importance in shaping the Appalachian highlands: U.S. Geological Survey Professional Paper, v. 1126-B, p. 17.

Hack, J. T., 1960, Interpretation of erosional topography in humid temperate regions: American Journal of Science, v. 258-A, p. 80-97.

Hadley, J.B. and Goldsmith, R., 1963, Geology of the eastern Great Smoky Mountains, North Carolina and Tennessee, U.S. Geological Survey professional paper 349-B, 118p.

Hamilton, W.B., 1961, Geology of the Richardson Cove and Jones Cove quadrangles, Tennessee, U.S. Geological Survey professional paper 349-A, 55p.

Harrison, C.G.A., 1994, Rates of continental erosion and mountain building: Geologische Rundschau, v. 83, no.2, p. 431-447.

Heimsath, A.M., Chappell, J., Spooner, N.A., and Questiaux, D.G., 2002, Creeping soil: Geology, v. 30, no. 2, p. 111-114.

Heimsath, A.M., Dietrich, W.E., Nishiizumi, K., Finkel, R.C., 2001, Stochastic processes of soil production and transport: erosion rates, topographic variation and cosmogenic nuclides in the Oregon Coast Range: Earth Surface Processes and Landforms, v. 26, p. 531-552.

Hovius, N., 1998, Controls on sediment supply by large rivers: in: Relative role of eustasy, climate, and tectonism in continental rocks, Society for Sedimentary Geology Special Publication, v. 59, p. 3-16.

Huvler, M.L., 1996, Post-orogenic denudation and mass-balanced topography of the Appalachian Mountain system from maturation indicators, thermochronology, and

metamorphic petrology: Geological Society of America, Abstracts with Programs, v. 28, no. 7, p. 500.

Judson, S., 1975, Evolution of the Appalachian topography, *in*: Melhorn, W.N. and Flemal, R.C., eds., Theories of landform development, Publications in Geomorphology, Bighamton, New York, p. 29-44.

Judson, S., 1968, Erosion of the land or what's happening to our continents: American Scientist, v. 56, p. 356-374.

Judson, S., and Ritter, D., 1964, Rates of regional denudation in the United States: Journal of Geophysical Research, v. 69, p. 3395-3401.

Kieth, A., 1895, Description of the Knoxville sheet (Tennessee-North Carolina): U.S. Geological Survey, Geological Atlas, Folio 16, 6p.

King, P. B., 1964, Geology of the central Great Smoky Mountains, Tennessee, U. S. Geological Survey Professional Paper: 1-148.

King, P. B., Neuman, R.B., and Hadley, J.B.,1968, Geology of the Great Smoky Mountains National Park, Tennessee and North Carolina: U. S. Geological Survey Professional Paper, 587, 23p.

Kirchner, J.W., Finkel, R.C., Riebe, C.S., Granger, D.E., Clayton, J.L., King, J.G., and Megahan, W.F., 2001, Mountain erosion over 10 yr, 10 ky and 10 My time scales: Geology, v. 29, no. 7, p. 591-594.

Kohl, C.P., and Nishiizumi, K., 1992, Chemical isolation of quartz for measurement of *in-situ* - produced cosmogenic nuclides: Geochimica et Cosmochimica Acta, v. 56, p. 3583-3587.

Lal, D., 1991, Cosmic ray labeling of erosion surfaces: *In situ* production rates and erosion models: Earth and Planetary Science Letters, v. 104, p. 424-439.

Lal, D., 1988, In situ-produced cosmogenic isotopes in terrestrial rocks: Annual Reviews of Earth and Planetary Science, v. 16, p. 355-388.

Lal, D., and Arnold, J.R., 1985, Tracing quartz through the environment: Proceedings of the Indian Academy of Science (Earth and Planetary Science), v. 94, p. 1-5.

Menard, H.W., 1961, Some rates of regional erosion: Journal of Geology, v. 69, p. 154-161.

Milliman, J.D., and Syvitski, P.M., 1992, Geomorphic/tectonic control of sediment discharge to the ocean: The importance of small mountainous rivers: The journal of Geology, v. 100, p. 525-544.

Mills, H.H., Brakenridge, G.R., Jacobson, R.B., Newell, W.l., Pavich, M.J., Pomeroy, J.S., 1987, Appalachian Mountains and plateaus, in Geomorphic Systems of North America (Graf, W.L., ed.), Geological Society of America, Centennial Special Volume 2, p. 5-50.

Naeser, N. D., Naeser, C.W., Kunk. D., Morgan, B.A. III, Schultz, A.P., Southworth, C.S., and Weems, R.E., 2001, Paleozoic through Cenozoic uplift, erosion, stream capture, and deposition history in the Valley and Ridge, Blue Ridge, Piedmont, and Coastal Plain province of Tennessee, North Carolina, Virginia, Maryland, and District of Columbia:

Geological Society of America, annual meeting, Abstracts with Programs, v. 33, no. 6, p. 312.

Naeser, N. D., Naeser, C.W., Morgan, B.A. III, Schultz, A.P., and Southworth, C.S., 1999, Paleozoic to Recent cooling history of the Blue Ridge Province, Virginia, North Carolina, and Tennessee, from apatite and zircon fission-track analysis: Geological Society of America, annual meeting, Abstracts with Programs, v. 31, no. 7, p. 117.

Nishiizumi, K., Winterer, E.L., Kohl, C.P., Klein, J., Middleton, R., Lal, D., and Arnold, J.R., 1989, Cosmic ray production rates of $^{10}$Be and $^{26}$Al in quartz from glacially polished rocks: Journal of Geophysical Research, v. 94, p. 17907-17915.

Pavich, M.J., 1985, Appalachian Piedmont morphogenesis: weathering, erosion and Cenozoic uplift, *in* Morisawa, M., and Hack, J.T., eds., Tectonic Geomorphology, Proceedings of the 15th annual Binghamton geomorphology symposium: Boston, Unwin Hyman, p. 299-319.

Pazzaglia, F.J. and Gardner, T.W., 2000, Late Cenozoic landscape evolution of the US Atlantic passive margin: insights into a North Aerican Great Escarpment, *in*: Summerfield, M.A., ed., Geomorphology and Global Tectonics: Chichester, John Wiley, p. 283-303.

Pazzaglia, F.J. and Brandon, M. T., 2001, A fluvial record of long-term steady-state uplift and erosion across the Cascadia forearc high, western Washington State: American Journal of Science, v. 301, no. 4-5, p. 385-431.

Pazzaglia, F. J. and Brandon, M. T., 1996, Macrogeomorphic evolution of the post-Triassic Appalachian Mountains determined by deconvolution of the offshore basin sedimentary record: Basin Research, v. 8, p. 255-278.

Pinet, P., and Souriau, M., 1988, continental erosion and large scale relief: Tectonics, v. 7, no. 3, p. 563-582.

Poag, C.W., and Sevon, W.D., 1989, A record of Appalachian denudation in postrift Mesozoic and Cenozoic sedimentary deposits of the U.S. middle Atlantic continental margin: Geomorphology, v. 2, p. 119-157.

Riebe, C.S., Kirchner, J.W., Granger, D.E., and Finkel, R.C., 2000, Erosional equilibrium and disequilibrium in the Sierra Nevada, inferred from cosmogenic $^{26}$Al and $^{10}$Be in alluvial sediments: Geology, v. 28, no. 9, p. 803-806.

Riebe, C.S., Kirchner, J.W., Granger, D.E., and Finkel, R.C., 2001, Minimal climatic control on erosion rates in the Sierra Nevada, California: Geology, v. 29, no. 5, p. 447-450.

Roden, M. K. and Miller, D. S., 1989, Apatite fission-track thermochronology of the Pennsylvania Appalachian basin: Geomorphology, v. 2, p. 39-51.

Schaller, M., von Blanckenburg, F., Hovius, N., and Kubik, P.W., 2001, Large scale erosion rates form in situ-produced cosmogenic nuclides in European river sediments: Earth and Planetary Science Letters, v. 188, p. 441-458.

Schumm, S.A., 1963, the disparity between present rates of denudation and orogeny: U.S. Geological Survey Professional Paper, 454-H, 13 p.

Slingerland, R. and Furlong, K. P., 1989, Geodynamic and geomorphic evolution of the Permo-Triassic Appalachian Mountains: Geomorphology, v. 2, p. 23-37.

Small, E.E., Anderson, R.S., and Hancock, G.S., 1999, Estimates of the rate of regolith production using $^{10}$Be and $^{26}$Al from an alpine hillslope: Geomorphology, v. 27, p. 131-150.

Stone, J., 2000, Air pressure and cosmogenic isotope production: Journal of Geophysical Research, v. 105, no. B10, p. 23753-23759.

Summerfield M.A., and Hulton, N.J., 1994, Natural controls of fluvial denudation rates in major world drainage basins: Journal of Geophysical Research, v. 99, no. B7, p. 13871-13883.

Sutter, J. F., Ratcliffe, N. M., and Musaka, S. B., 1985, $^{40}$Ar/$^{39}$Ar and K-Ar data bearing on the metamorphic and tectonic history of western New England: Geological Society of America Bulletin, v. 96, p. 123-136

Whipple, K.X., 2001, Fluvial landscape response time; how plausible is steady state denudation?: American Journal of Science, v. 301, no. 4-5, p. 313-325.

Zen, E., 1991, Phanerozoic denudation history of the southern New England Appalachians deduced from pressure data: American Journal of Science, v. 291, p. 401-424.

Zimmerman, R. A., 1979, Apatite fission track age evidence of post-Triassic uplift in the central and southern Appalachians: Geological Society of America Abstracts with Programs, v. 11, p. 219.

## FIGURE CAPTIONS

Figure 1. Location map. GRSM – Great Smoky Mountains. Gray line – boundary of Great Smoky Mountains National Park. Thick dashed line – divides between major river systems in the region. Thin dashed line – GRSM main drainage divide.

Figure 2. A. View upstream of the Big Creek drainage system. Ridge tops are flat and are connected to the deeply incised rivers by steep slopes. Ridge tops and slopes are totally vegetated. B. Tree throw exposes sandy soil along the main Great Smoky mountain water divide (beside the Appalachian Trail). C. Typical pool in Great Smoky Mountain stream (Abrams Creek). Sediment from pools like this was sampled. D. Sediment was also sampled from sand bars such as the one in the foreground (Big Creek). E. The soil mantle covers the entire slope environment, from the alluvial channel to the ridge tops. Soil section in photo is exposed along the Great Smoky Mountain main drainage divide due to compaction along the Appalachian Trail. F. Bedrock outcrop of Thunderhead Formation sandstone along the Great Smoky Mountain main drainage divide (1 mile northeast of Newfound Gap). The outcrops along the divide rise 1-4 meters above their

surrounding. G. The Cosby Fan area. The surface of the fan is seen in the foreground dissected by active channels. The Great Smoky Mountain northern front is in the background.

Figure 3. Geologic map of the Great Smoky Mountains. Only main lithologies are shown. Most of the range is underlain by quartz bearing rocks. Geology after Hadley and Goldsmith, 1963; King, 1964; Hamilton, 1961; King et al., 1968.

Figure 4. Sampling locations in the Great Smoky Mountains. Numbers under sample names are model erosion rates (m $My^{-1}$) calculated from $^{10}Be$ activities.

Figure 5. Detailed tributary sampling in the Oconaluftee River (A), Raven Fork (A), and Little River (B). Numbers under sample name are erosion rates in m $My^{-1}$ calculated from $^{10}Be$ activities. Samples GSRF-2, GSRF-3, GSRF-5, and GSRF-7 were collected from the Ledge Creek sub basin. Samples GSRF-6, GSRF-8, GSRF-9, and GSRF-10 were collected from the Straight Fork sub basin.

Figure 6. $^{10}Be$ activities of colluvium samples and their relation to $^{10}Be$ activities of the source outcrop. Shaded bars – bedrock $^{10}Be$ activity. Open bars – colluvium $^{10}Be$ activity. Colluvium $^{10}Be$ activities can be higher, equal, or lower than $^{10}Be$ activities of the source outcrop.

Figure 7. Results of $^{10}Be$ analysis of grain size tests in alluvial sediments in the Great Smoky Mountains. Fraction size (mm) written in column. Sample name written below horizontal axis. A. $^{10}Be$ activities in large fractions (2-10, >10 mm and >2 mm in samples GSCO-1 and GSCO-7) are lower suggesting shorter dosing history or/and lower production rates. $\Delta P$ – the difference between the basin-wide effective production rate and the sampling location production rate. Higher $\Delta P$ reflects greater relief in the sampled basin. B. Erosion rates calculated from $^{10}Be$ activities using basin-wide production rates for all size fractions. This calculation results in the apparent high erosion rates of the large clasts. The greater $\Delta P$ is, the greater the difference between the calculated erosion rates of the larger and smaller size fractions. Normalized $^{10}Be$ activities were calculated using high latitude sea level production rate of 5.17 $^{10}Be$ atoms $g^{-1}$ quartz $yr^{-1}$. C. Erosion rates calculated from $^{10}Be$ activities using basin-wide production rates for the small grain sizes (which are derived from the entire basin) and sampling location production rate for the large grain sizes (which are derived from the lower parts of the adjacent slopes). Except for two cases (>10 mm in GSLR-7 and 2-10 mm in GSCO-1A), erosion rates of all sizes are similar within each sampling site.

Figure 8. Longitudinal profiles of the sampled rivers in the Great Smoky Mountains. Topography digitized from 1:24000 topographic maps. Knick point location can be correlated to out crop of resistant rock. In some cases there is no apparent lithologic or structural reasin for the existence of the knock point. Intraformational variations in resistance to erosion can explain such knick points. None of the longitudinal profiles

suggest recent activity of the faults crossed by the streams. Geology after Hadley and Goldsmith, 1963; King, 1964; Hamilton, 1961; King et al., 1968.

Figure 9. $^{10}$Be normalized activities (non-linear scale) and $^{10}$Be model erosion rates plotted against various Great Smoky Mountain drainage basin physical parameters. A. A weak correlation between erosion rates and basin maximum elevation. B. No correlation between erosion rates and basin relief (elevation difference between highest point in the basin and the sampling location). C. No correlation between erosion rates and drainage basin relief ratio. Relief ratio is defined as the ratio between the maximum relief and the length of main stem river draining the basin. D. No correlation between erosion rates and drainage basin area. However, the average erosion rate of the headwater basins (27.6±7.4 m $My^{-1}$, n=18), the outlet rivers (24.3±5.6 m $My^{-1}$, n=15), and the largest river in the Great Smoky Mountains (26.3±5.2 m $My^{-1}$) are similar indicating the thorough mixing and the rapid movement of sediment in the alluvial channel and suggesting the uniform average erosion of all parts of the alluvial system. E. Drainage basin average elevation and rates of erosion are not correlated. F. Erosion rates are not correlated with the distance from the western end of the mountain range. Most of the precipitation in the Great Smoky Mountains is generated from storms approaching from the northwest. A correlation with the distance from the western end of the mountain range and the source of precipitation would have suggested a climatic control over erosion rates. G. Rates of erosion are correlated with the mean slope gradient in each drainage basin indicating the importance of slope processes in determining erosion rates in the Great Smoky Mountains. H. No correlation between drainage density (km length of channels per $km^2$ of basin area) and erosion rates.

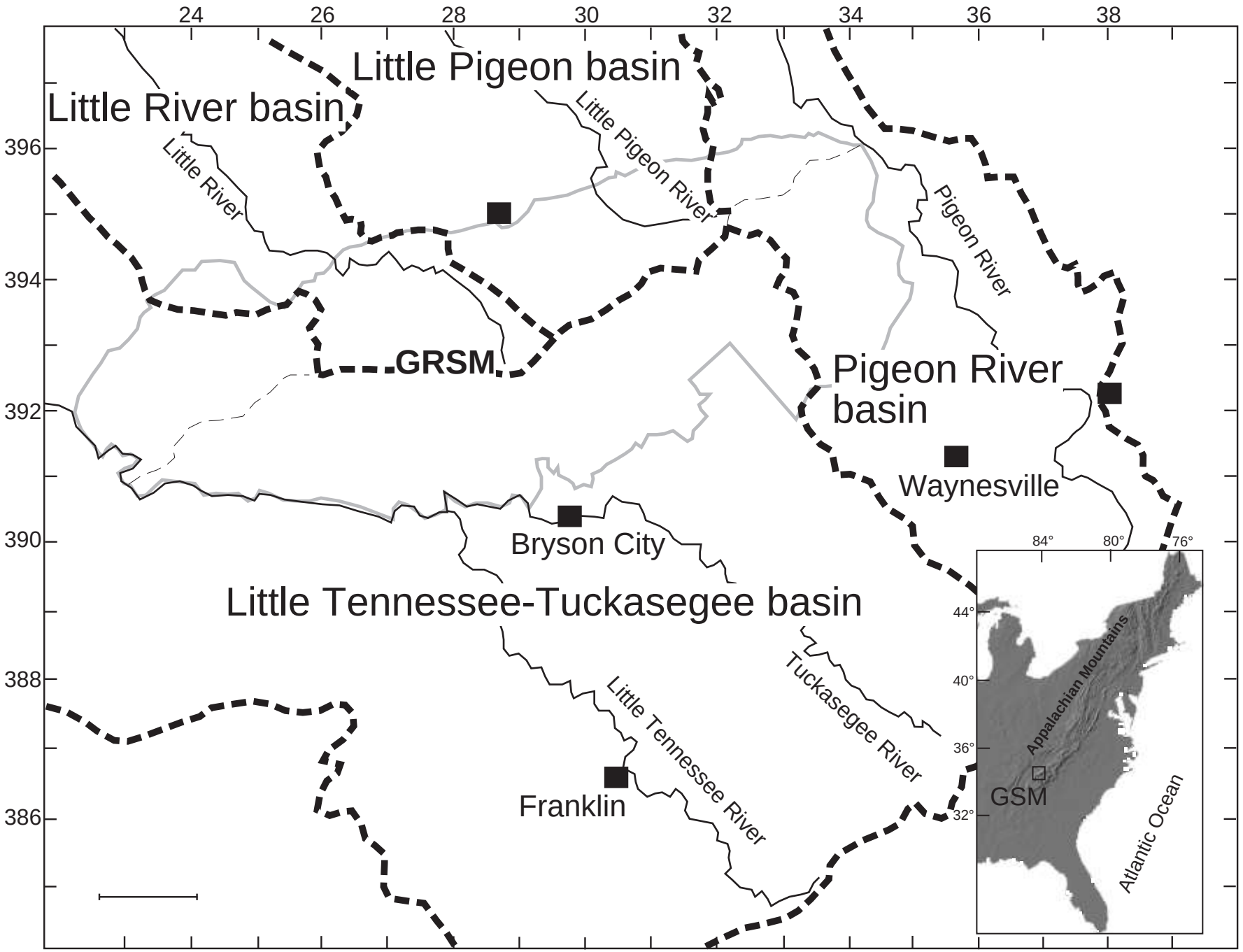
24
26
28
30
32
34
36
38
396
394
392
390
388
386
Little Pigeon basin
Little River basin
Little River
Little Pigeon River
Pigeon River
GRSM
Pigeon River basin
Waynesville
Bryson City
Little Tennessee-Tuckasegee basin
Tuckasegee River
Little Tennessee River
Franklin
84°
80°
76°
44°
40°
36°
32°
Appalachian Mountains
GSM
Atlantic Ocean

A

B

C

D

E

F


G

Matmon et al., figure 2

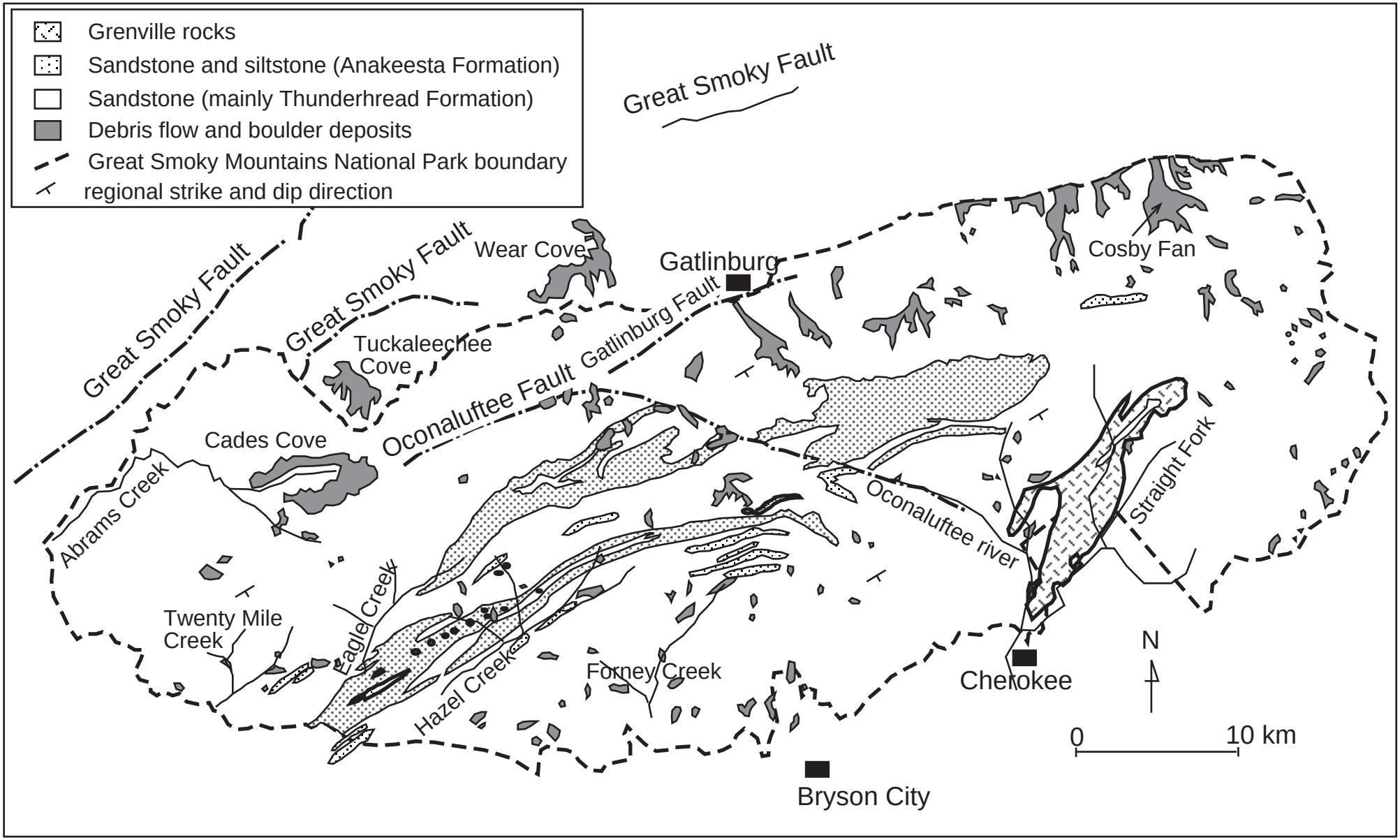


Matmon et al., figure 3

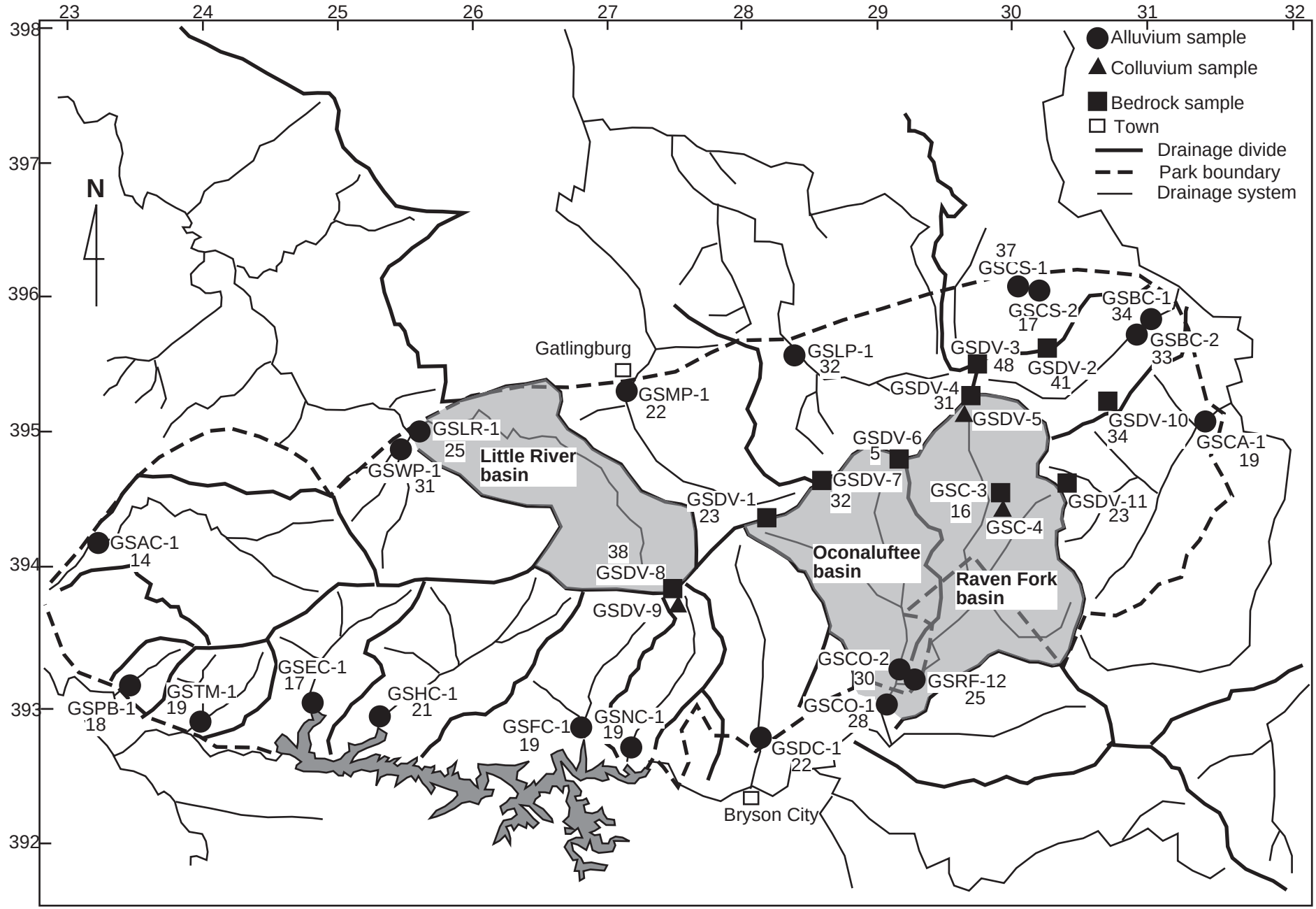


Matmon et al., figure 4

A

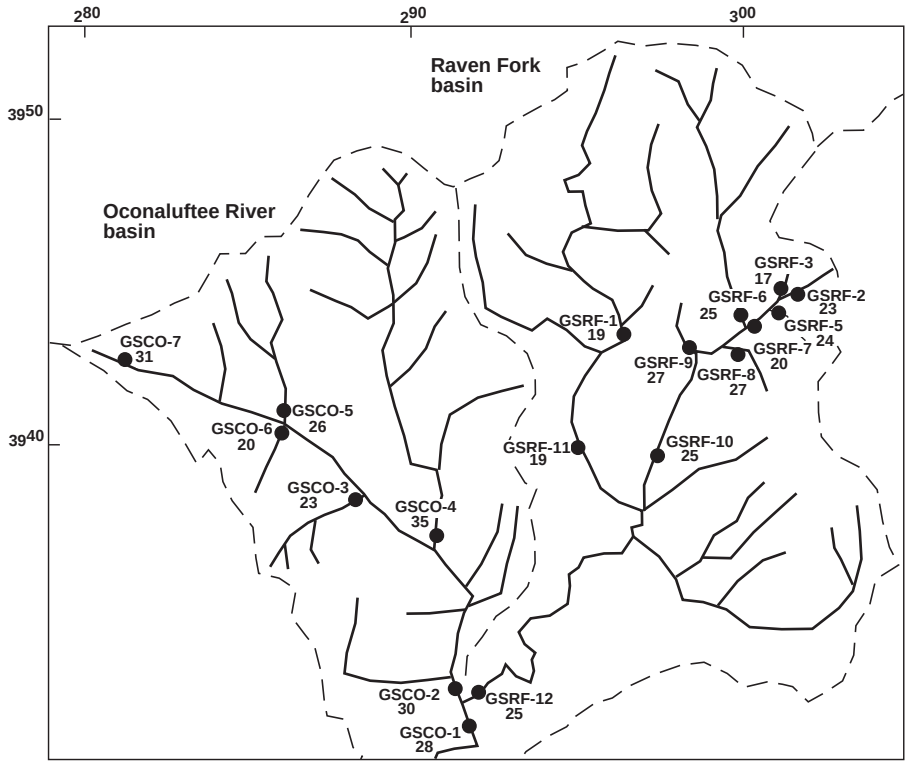


B

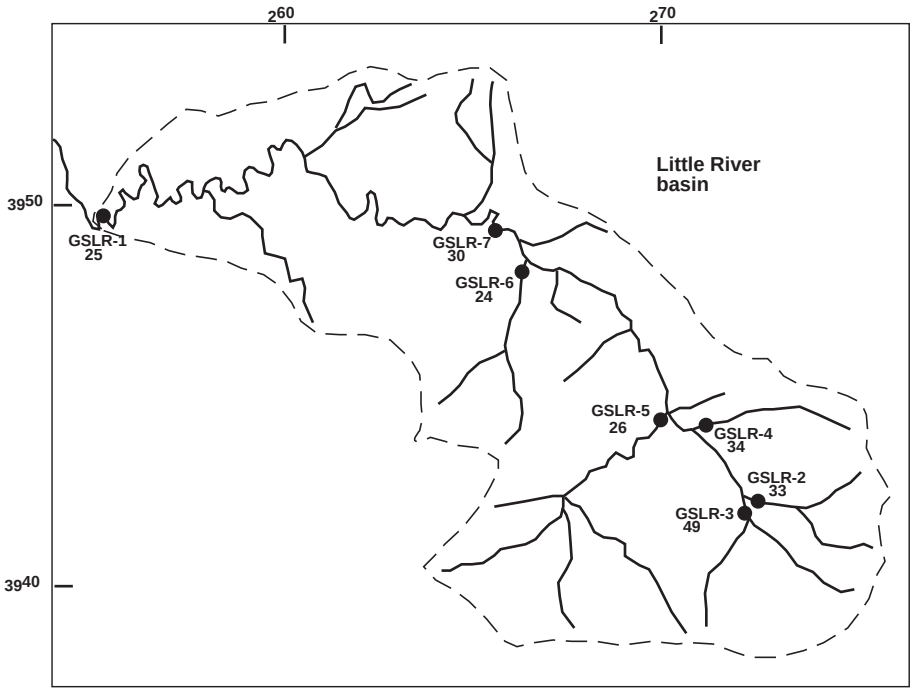


Matmon et al., Fig. 5

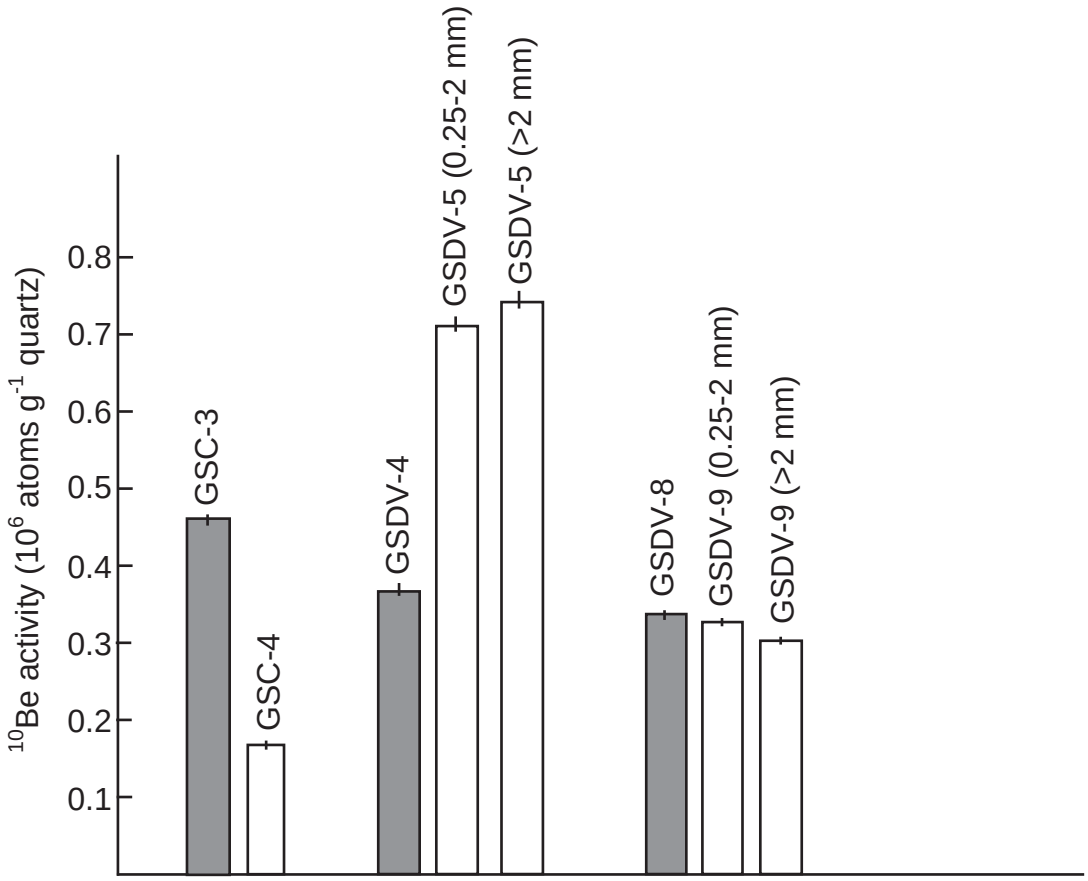


Matmon et al., figure 6

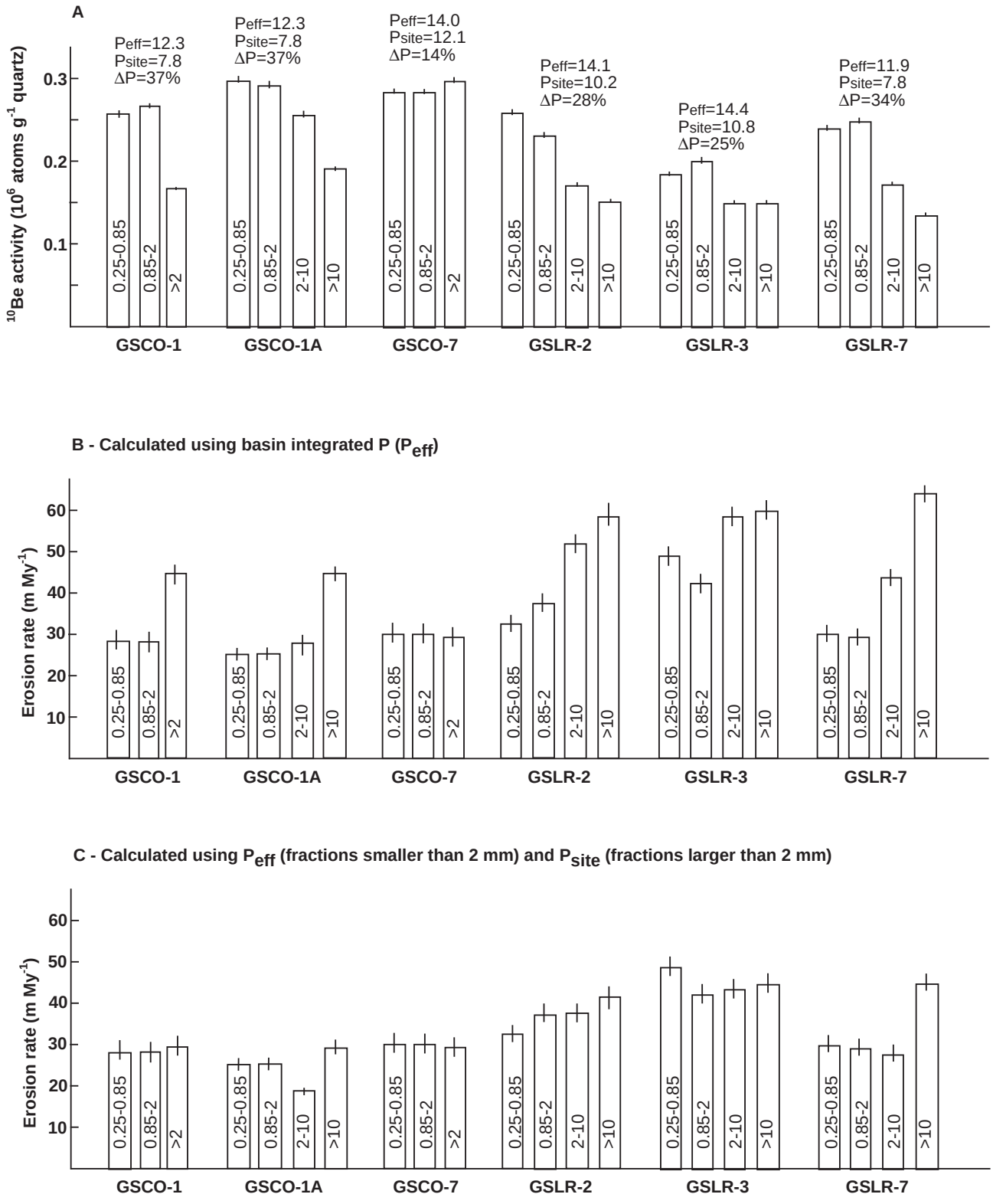


Matmon et al., figure 7

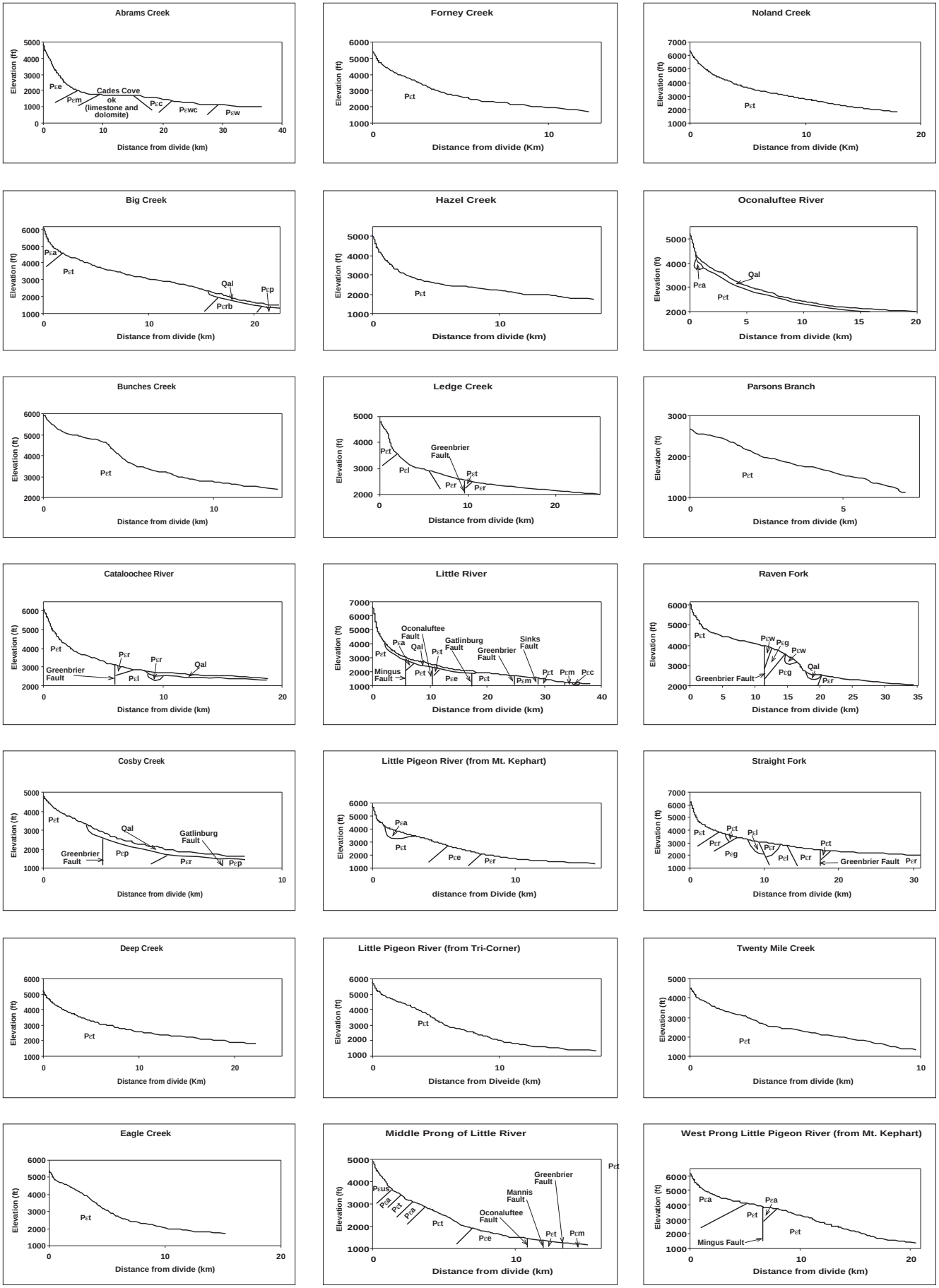


| | | | |
|---|---|---|---|
| **Pεe** | **- Elkmont sandstone** | **Qal** | **- Quaternary? alluvium** |
| **Pεm** | **- Metcalf phyllite** | **Pεp** | **- Pigeon siltstone and sandstone** |
| **Pεc** | **- Cades sandstone** | **Pεr** | **- Roaring Fork sandstone** |
| **Pεwc** | **- Wilhite shale** | **Pεu** | **- Un-named sandstone** |
| **Pεw** | **- Wading Branch graywacke and conglomerate** | **Pεg** | **- Grenville basement complex** |
| **Pεa** | **- Anakeesta slate, sandstone, and conglomerate** | **Pεl** | **- Long Arm quartzite** |
| **Pεt** | **- Thunderhead sandstone** | **Pεrb** | **- Rich Butt sandstone** |

Matmon et al., figure 8

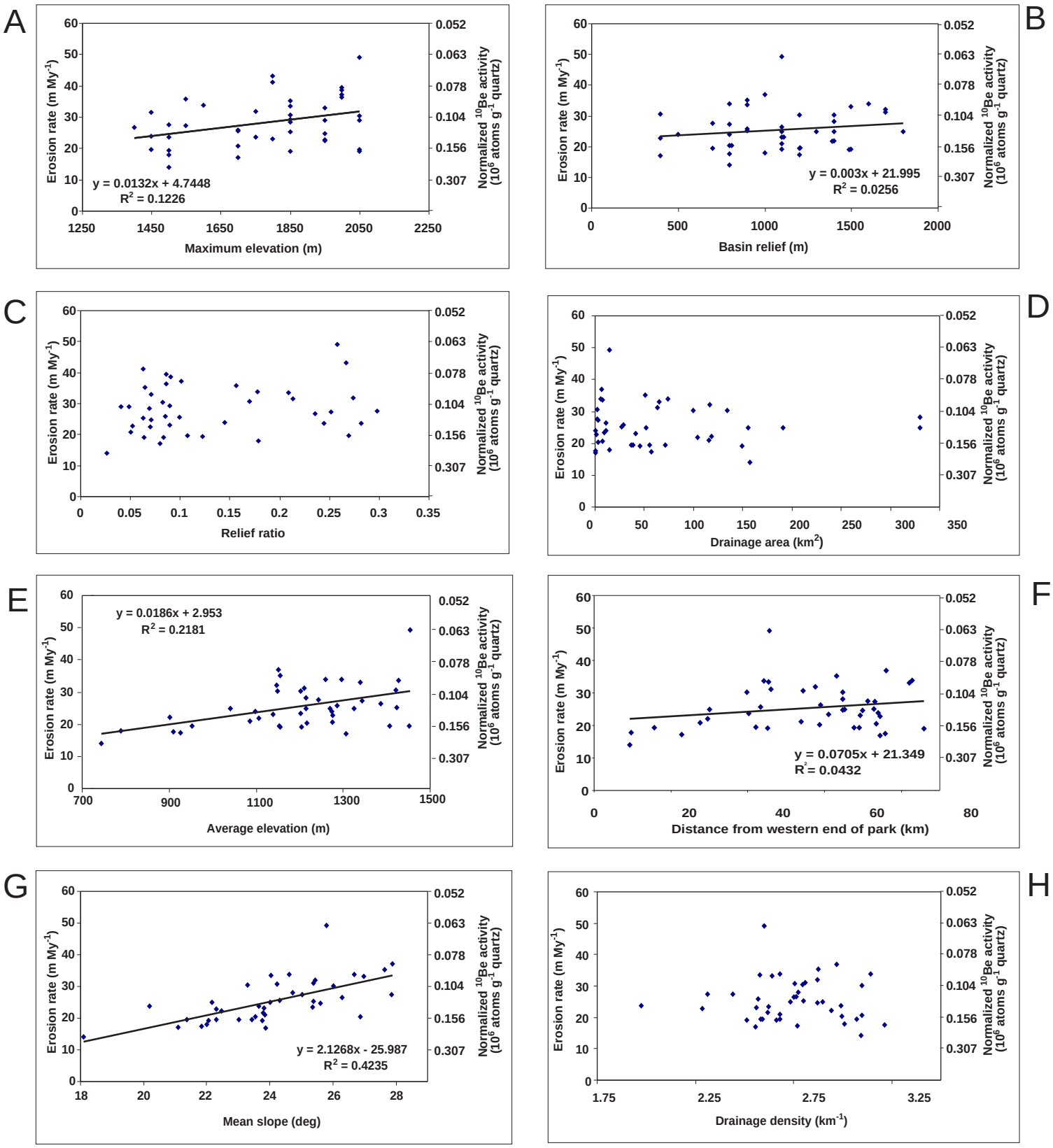


Matmon et al., figure 9

Table 1

*Sample locations – Great Smoky Mountains*

| Sample name | Basin name | Longitude (UTM)[1] | Latitude (UTM)[1] | Sampling elevation (m asl)[2] | Basin area ($km^2$)[3] | Sample type |
|---|---|---|---|---|---|---|
| GSRF-1 | Raven Fork | 0295743 | 3942840 | 1090 | 36.9 | Sediment |
| GSRF-2 | Ledge Creek | 0301349 | 3944775 | 1100 | 1.4 | Sediment |
| GSRF-3 | Ledge Creek | 0301349 | 3944775 | 1100 | 1.0 | Sediment |
| GSRF-5 | Ledge Creek | 0300781 | 3944187 | 1030 | 1.0 | Sediment |
| GSRF-6 | Straight Fork | 0299677 | 3944114 | 960 | 27.3 | Sediment |
| GSRF-7 | Ledge Creek | 0299969 | 3943633 | 980 | 7.7 | Sediment |
| GSRF-8 | Straight Fork | 0299518 | 3943186 | 940 | 3.6 | Sediment |
| GSRF-9 | Straight Fork | 0298548 | 3942529 | 910 | 2.9 | Sediment |
| GSRF-10 | Straight Fork | 0297176 | 3939957 | 920 | 51.9 | Sediment |
| GSRF-11 | Raven Fork | 0294868 | 3939549 | 800 | 55.7 | Sediment |
| GSRF-12 | Raven Fork | 0291862 | 3932549 | 630 | 191.5 | Sediment |
| GSRF-13 | Bunches Creek | 0296372 | 3937337 | 760 | 42 | Sediment |
| GSCO-1 | Oconaluftee | 0291319 | 3931360 | 640 | 330.2 | Sediment |
| GSCO-1A | Oconaluftee | 0291319 | 3931360 | 640 | 330.2 | Sediment |
| GSCO-2 | Oconaluftee | 0290852 | 3932532 | 640 | 134.9 | Sediment |
| GSCO-3 | Oconaluftee | 0290710 | 3932985 | 650 | 9.4 | Sediment |
| GSCO-4 | Oconaluftee | 0290398 | 3937215 | 700 | 51.4 | Sediment |
| GSCO-5 | Oconaluftee | 0288276 | 3938250 | 740 | 11.6 | Sediment |
| GSCO-6 | Oconaluftee | 0286247 | 3940454 | 870 | 3.3 | Sediment |
| GSCO-7 | Oconaluftee | 0281413 | 3942223 | 1230 | 2.3 | Sediment |
| GSLR-1 | Little River | 0254927 | 3949542 | 360 | 155.8 | Sediment |
| GSLR-2 | Little River | 0272163 | 3942248 | 990 | 8 | Sediment |
| GSLR-3 | Little River | 0272081 | 3942329 | 1070 | 15 | Sediment |
| GSLR-4 | Little River | 0270849 | 3944114 | 920 | 6 | Sediment |
| GSLR-5 | Little River | 0269757 | 3944107 | 870 | 30 | Sediment |
| GSLR-6 | Little River | 0266234 | 3948211 | 670 | 12 | Sediment |
| GSLR-7 | Little River | 0265313 | 3949634 | 640 | 100 | Sediment |
| GSBC-1 | Big Creek | 0308730 | 3958027 | 500 | 74.8 | Sediment |
| GSBC-2 | Big Creek | 0307342 | 3956512 | 730 | 65.7 | Sediment |
| GSCS-1 | Cosby Creek | 0300560 | 3958663 | 700 | 7.1 | Sediment |
| GSCS-2 | Cosby Creek | 0300529 | 3958622 | 700 | 0.8 | Sediment |
| GSLP-1 | Little Pigeon | 0281639 | 3957206 | 430 | 117.3 | Sediment |
| GSMP-1 | Middle Prong | 0254696 | 3949286 | 360 | 118.3 | Sediment |
| GSWP-1 | West Prong | 0270544 | 3952039 | 500 | 63.6 | Sediment |
| GSDC-1 | Deep Creek | 0279101 | 3927035 | 560 | 104.9 | Sediment |
| GSAC-1 | Abram's Creek | 0234078 | 3944424 | 350 | 158 | Sediment |
| GSPB-1 | Parsons Branch | 0233897 | 3932192 | 430 | 15 | Sediment |
| GSTM-1 | Twenty Mile | 0238819 | 3928425 | 380 | 39 | Sediment |
| GSNC-1 | Nolan Creek | 0270636 | 3926601 | 590 | 47 | Sediment |
| GSCA-1 | Cataluchee River | 0312519 | 3949004 | 810 | 150 | Sediment |
| GSFC-1 | Forney Creek | 0267061 | 3927518 | 690 | 72 | Sediment |
| GSHC-1 | Hazel Creek | 0253395 | 3928378 | 550 | 116 | Sediment |

| Sample name | Basin name | Longitude (UTM) | Latitude (UTM) | Sampling elevation (masl) | Basin area ($km^2$) | Sample type |
|---|---|---|---|---|---|---|
| GSEC-1 | Eagle Creek | 0248544 | 3930507 | 570 | 58 | Sediment |
| GSC-3 | Straight Fork | 0297169 | 3943423 | 1250 | NA | Rock - Gneiss |
| GSC-4 | Straight Fork | 0297169 | 3943423 | 1250 | NA | Coluvium - Colluvium below GSC-3 |
| GSDV-1 | Oconaluftee, Little Pigeon | 0280685 | 3943354 | 1620 | NA | Rock - Thunderhead Sandstone |
| GSDV-2 | Big Creek, Cosby Creek | 0302099 | 3955965 | 1570 | NA | Rock - Thunderhead Sandstone |
| GSDV-3 | Big Creek, Cosby Creek | 0297600 | 3955750 | 1750 | NA | Rock - Thunderhead Sandstone |
| GSDV-4 | Big Creek, Raven Fork, Little Pigeon | 0294992 | 3951532 | 1900 | NA | Rock - Thunderhead Sandstone |
| GSDV-5 | Big Creek, Raven Fork, Little Pigeon | 0294668 | 3951460 | 1900 | NA | Colluvium - Colluvium around GSDV-4 |
| GSDV-6 | Raven Fork, Little Pigeon | 0292299 | 3948553 | 1800 | NA | Rock - Quartz pegmatite |
| GSDV-7 | Oconaluftee, Little Pigeon | 0284339 | 3945833 | 1700 | NA | Rock - Anakeesta Sandstone |
| GSDV-8 | Little River, Nolan Creek, Forney Creek | 0273137 | 3938070 | 2010 | NA | Rock - Thunderhead Sandstone |
| GSDV-9 | Little River, Nolan Creek, Forney Creek | 0273331 | 3938095 | 2030 | NA | Colluvium - Colluvium around GSDV-8 |
| GSDV-10 | Mt. Sterling Big Creek, Cataloochee Creek | 0307713 | 3952348 | 1750 | NA | Rock - Thunderhead Sandstone |
| GSDV-11 | Ledge Creek, Cataloochee Creek | 0302505 | 3945542 | 1410 | NA | Rock - Roaring Fork Sandstone |

[1] Measured with Garmin 12; referenced to NAD 27; [2] Measured with (GPS type); referenced to NAD 27; [3] area upstream of sampling point; NA – not applicable.

Table 2

*Cosmogenic results of Great Smoky Mountain bedrock and colluvial samples*

| Sample name | Measured $^{10}$Be ($10^6$ atoms g$^{-1}$)[1] | Measured $^{26}$Al ($10^6$ atoms g$^{-1}$)[1] | $^{26}$Al/$^{10}$Be | $^{10}$Be (SL,>60°) ($10^6$ atoms g$^{-1}$)[2] | $^{26}$Al (SL,>60°) ($10^6$ atoms g$^{-1}$)[2] | Production factor[3] |
|---|---|---|---|---|---|---|
| GSC-3 (B) | 0.470±0.015 | 2.797±0.131 | 5.95±0.32 | 0.197±0.005 | 1.169±0.055 | 2.39 |
| GSC-4 | 0.173±0.012 | 1.069±0.069 | 6.17±0.48 | 0.073±0.003 | 0.447±0.029 | 2.39 |
| GSDV-1 (B) | 0.431±0.008 | 2.536±0.139 | 5.89±0.39 | 0.138±0.005 | 0.812±0.044 | 3.12 |
| GSDV-2 (B) | 0.221±0.008 | 0.000±0.000 | 0.00±0.00 | 0.077±0.003 | 0.000±0.000 | 2.98 |
| GSDV-3 (B) | 0.216±0.007 | 0.000±0.000 | 0.00±0.00 | 0.065±0.002 | 0.000±0.000 | 3.44 |
| GSDV-4 (B) | 0.371±0.018 | 0.000±0.000 | 0.00±0.00 | 0.101±0.005 | 0.000±0.000 | 3.95 |
| [4] (0.25-2) GSDV-5 | 0.726±0.020 | 4.906±0.236 | 6.75±0.38 | 0.197±0.005 | 1.332±0.064 | 3.68 |
| [4] (>2) GSDV-5 | 0.755±0.023 | 4.692±0.226 | 6.21±0.36 | 0.205±0.006 | 1.274±0.061 | 3.68 |
| GSDV-6 (B) | 2.169±0.066 | 0.000±0.000 | 0.00±0.00 | 0.635±0.019 | 0.000±0.000 | 3.68 |
| GSDV-7(B) | 0.297±0.008 | 0.000±0.000 | 0.00±0.00 | 0.097±0.003 | 0.000±0.000 | 3.20 |
| GSDV-8 (B) | 0.346±0.013 | 2.324±0.114 | 6.71±0.42 | 0.083±0.003 | 0.559±0.027 | 4.23 |
| [4] (0.25-2) GSDV-9 | 0.333±0.011 | 2.145±0.115 | 6.44±0.40 | 0.079±0.003 | 0.508±0.027 | 4.23 |
| [4] (>2) GSDV-9 | 0.305±0.010 | 2.142±0.118 | 7.02±0.45 | 0.072±0.002 | 0.507±0.028 | 4.23 |
| GSDV-10 (B) | 0.302±0.010 | 0.000±0.000 | 0.00±0.00 | 0.092±0.003 | 0.000±0.000 | 3.44 |
| GSDV-11 (B) | 0.410±0.013 | 2.394±0.112 | 5.84±0.33 | 0.158±0.005 | 0.923±0.043 | 2.78 |

[1] Errors are 1σ uncertainties in analytical measurements (AMS, ICP); [2] Using sea level, high latitude production rate of 5.17 $^{10}$Be atoms g$^{-1}$ quartz yr$^{-1}$ (Bierman et al., 1996; Stone, 2000; Gosse and Stone, 2001); [3] Production factor is the ratio between the site production rate (using Lal, 1991 for elevation/latitude correction without muon production) and sea level, >60° latitude production rate; [4] Grain size in mm. (B) – bedrock samples. Unmarked samples are colluvium samples.

Table 3 *Great Smoky Mountain sediment samples*

| Sample name | Measured $^{10}$Be ($10^6$ atoms $g^{-1}$)[1] | Measured $^{26}$Al ($10^6$ atoms $g^{-1}$)[1] | $^{26}$Al/$^{10}$Be | $^{10}$Be (SL,>60°) ($10^6$ atoms $g^{-1}$)[2] | $^{26}$Al (SL,>60°) ($10^6$ atoms $g^{-1}$)[2] | Production factor[3] |
|---|---|---|---|---|---|---|
| GSRF-1 (T) | 0.434±0.011 | 2.460±0.120 | 5.66±0.31 | 0.1614±0.0043 | 0.914±0.045 | 2.69 |
| GSRF-2 (T) | 0.335±0.009 | 1.868±0.089 | 5.58±0.30 | 0.1372±0.0035 | 0.766±0.037 | 2.44 |
| GSRF-3 (T) | 0.461±0.012 | 2.522±0.133 | 5.47±0.32 | 0.1839±0.0050 | 1.006±0.053 | 2.51 |
| GSRF-5 (T) | 0.322±0.009 | 2.040±0.100 | 6.33±0.36 | 0.1316±0.0037 | 0.833±0.041 | 2.45 |
| GSRF-6 (T) | 0.341±0.009 | 1.814±0.085 | 5.31±0.29 | 0.1246±0.0035 | 0.662±0.031 | 2.74 |
| GSRF-7 (T) | 0.376±0.011 | 2.150±0.124 | 5.72±0.37 | 0.1529±0.0044 | 0.875±0.051 | 2.46 |
| GSRF-8 (T) | 0.297±0.009 | 1.331±0.102 | 4.49±0.37 | 0.1150±0.0034 | 0.516±0.040 | 2.58 |
| GSRF-9 (T) | 0.274±0.008 | 1.694±0.090 | 6.18±0.37 | 0.1143±0.0033 | 0.706±0.037 | 2.40 |
| GSRF-10 (T) | 0.325±0.009 | 1.897±0.105 | 5.84±0.36 | 0.1270±0.0035 | 0.741±0.041 | 2.56 |
| GSRF-11 (T) | 0.452±0.011 | 2.675±0.131 | 5.92±0.32 | 0.1616±0.0040 | 0.956±0.047 | 2.80 |
| GSRF-12 (B) | 0.310±0.009 | 1.533±0.082 | 4.94±0.30 | 0.1259±0.0036 | 0.622±0.033 | 2.47 |
| GSRF-13 (T) | 0.300±0.010 | 0.000±0.000 | 0.00±0.00 | 0.136±0.004 | 0.000±0.000 | 2.24 |
| GSCO-1 (B) | 0.264±0.010 | 1.477±0.084 | 5.58±0.39 | 0.1118±0.0043 | 0.624±0.036 | 2.37 |
| GSCO-1A (B) | 0.295±0.009 | 1.537±0.093 | 5.21±0.35 | 0.126±0.004 | 0.658±0.040 | 2.37 |
| GSCO-2 (B) | 0.234±0.007 | 1.317±0.068 | 5.64±0.34 | 0.1039±0.0032 | 0.586±0.030 | 2.25 |
| GSCO-3 (T) | 0.312±0.008 | 1.785±0.085 | 5.72±0.31 | 0.1338±0.0033 | 0.765±0.037 | 2.34 |
| GSCO-4 (T) | 0.200±0.006 | 1.062±0.094 | 5.30±0.49 | 0.0893±0.0025 | 0.473±0.042 | 2.25 |
| GSCO-5 (T) | 0.317±0.008 | 1.848±0.088 | 5.83±0.32 | 0.1191±0.0032 | 0.694±0.033 | 2.67 |
| GSCO-6 (T) | 0.361±0.012 | 2.110±0.111 | 5.85±0.37 | 0.1542±0.0051 | 0.902±0.048 | 2.34 |
| GSCO-7 (T) | 0.278±0.007 | 1.724±0.094 | 6.20±0.38 | 0.102±0.003 | 0.636±0.035 | 2.71 |
| GSLR-1 (B) | 0.264±0.007 | 1.614±0.090 | 6.11±0.38 | 0.1261±0.0034 | 0.771±0.043 | 2.10 |
| GSLR-2 (T) | 0.256±0.008 | 1.404±0.088 | 5.48±0.38 | 0.094±0.003 | 0.514±0.032 | 2.76 |
| GSLR-3 (T) | 0.178±0.006 | 0.000±0.000 | 0.00±0.00 | 0.064±0.002 | 0.000±0.000 | 2.81 |
| GSLR-4 (T) | 0.224±0.007 | 0.000±0.000 | 0.00±0.00 | 0.093±0.003 | 0.000±0.000 | 2.43 |
| GSLR-5 (T) | 0.301±0.009 | 0.000±0.000 | 0.00±0.00 | 0.122±0.004 | 0.000±0.000 | 2.48 |
| GSLR-6 (T) | 0.282±0.010 | 0.000±0.000 | 0.00±0.00 | 0.132±0.005 | 0.000±0.000 | 2.16 |

Table 3 (cont.)

| Sample name | Measured $^{10}$Be ($10^6$ atoms $g^{-1}$)[1] | Measured $^{26}$Al ($10^6$ atoms $g^{-1}$)[1] | $^{26}$Al/$^{10}$Be | $^{10}$Be (SL,>60°) ($10^6$ atoms $g^{-1}$)[2] | $^{26}$Al (SL,>60°) ($10^6$ atoms $g^{-1}$)[2] | Production factor[3] |
|---|---|---|---|---|---|---|
| GSLR-7 (B) | 0.240±0.008 | 0.000±0.000 | 0.00±0.00 | 0.104±0.003 | 0.000±0.000 | 2.35 |
| GSBC-1 (B) | 0.234±0.006 | 1.454±0.091 | 6.22±0.42 | 0.0929±0.0025 | 0.577±0.036 | 2.52 |
| GSBC-2 (B) | 0.247±0.008 | 1.290±0.076 | 5.23±0.35 | 0.0949±0.0030 | 0.496±0.029 | 2.60 |
| GSCS-1 | 0.191±0.005 | 1.130±0.059 | 5.91±0.35 | 0.0851±0.0023 | 0.503±0.026 | 2.25 |
| GSCS-2 | 0.333±0.009 | 1.873±0.090 | 5.62±0.31 | 0.1785±0.0047 | 1.003±0.048 | 1.87 |
| GSDC-1 (B) | 0.316±0.008 | 1.759±0.090 | 5.57±0.32 | 0.1448±0.0038 | 0.806±0.041 | 2.19 |
| GSLP-1 (B) | 0.225±0.007 | 1.280±0.072 | 5.70±0.36 | 0.0985±0.0029 | 0.561±0.032 | 2.28 |
| GSMP-1 (B) | 0.267±0.007 | 1.366±0.065 | 5.12±0.28 | 0.1420±0.0038 | 0.727±0.035 | 1.88 |
| GSWP-1 (B) | 0.242±0.006 | 1.251±0.067 | 5.17±0.31 | 0.1010±0.0027 | 0.522±0.028 | 2.40 |
| GSAC-1 (B) | 0.362±0.011 | 0.000±0.000 | 0.00±0.00 | 0.222±0.007 | 0.000±0.000 | 1.66 |
| GSPB-1 (B) | 0.295±0.012 | 0.000±0.000 | 0.00±0.00 | 0.174±0.007 | 0.000±0.000 | 1.71 |
| GSTM-1 (B) | 0.309±0.009 | 0.000±0.000 | 0.00±0.00 | 0.161±0.005 | 0.000±0.000 | 1.95 |
| GSNC-1 (B) | 0.363±0.012 | 0.000±0.000 | 0.00±0.00 | 0.163±0.005 | 0.000±0.000 | 2.28 |
| GSCA-1 (B) | 0.379±0.011 | 0.000±0.000 | 0.00±0.00 | 0.163±0.005 | 0.000±0.000 | 2.35 |
| GSFC-1 (B) | 0.359±0.011 | 0.000±0.000 | 0.00±0.00 | 0.161±0.005 | 0.000±0.000 | 2.28 |
| GSHC-1 (B) | 0.318±0.010 | 0.000±0.000 | 0.00±0.00 | 0.150±0.005 | 0.000±0.000 | 2.15 |
| GSEC-1 (B) | 0.341±0.011 | 0.000±0.000 | 0.00±0.00 | 0.181±0.006 | 0.000±0.000 | 1.91 |

[1] Errors are 1σ uncertainties in analytical measurements (AMS, ICP); [2] Using basin-wide effective production rate (convolving hypsometric curves and Lal, 1991 for elevation/latitude correction without muon production); [3] Production factor is the ratio between the basin-wide effective production rate and sea level, >60° latitude production rate of 5.17 $^{10}$Be atoms $g^{-1}$ quartz $yr^{-1}$ (Bierman et al., 1996; Stone, 2000; Gosse and Stone, 2001); (B) Outlet rivers of the Great Smoky Mountains. (T) Tributary of Oconaluftee River (GSCO), Raven Fork (GSRF), and Little River (GSLR). All sediment samples were analyzed using the 0.25-0.85 mm grain size.

Table 4

*Cosmogenic results of grain size test samples, Great Smoky Mountains*

| Sample name | Size fraction (μm) | Measured $^{10}$Be ($10^6$ atoms g$^{-1}$) [1] | Measured $^{26}$Al ($10^6$ atoms g$^{-1}$) [1] | $^{26}$Al/$^{10}$Be | $^{10}$Be (SL,>60°) ($10^6$ atoms g$^{-1}$)[2] | $^{26}$Al (SL,>60°) ($10^6$ atoms g$^{-1}$)[2] | Production factor[3] |
|---|---|---|---|---|---|---|---|
| GSCO-1 (B) | 250-850 | 0.264±0.010 | 1.477±0.084 | 5.58±0.39 | 0.1118±0.0043 | 0.624±0.036 | 2.37 |
| GSCO-1 (B) | 850-2000 | 0.266±0.007 | 1.461±0.079 | 5.50±0.33 | 0.1123±0.0029 | 0.618±0.033 | 2.37 |
| GSCO-1 (B) | >2000 | 0.165±0.004 | 0.961±0.051 | 5.81±0.35 | 0.0699±0.0019 | 0.406±0.022 | 2.37 |
| GSCO-1A (B) | 250-850 | 0.295±0.009 | 1.537±0.093 | 5.21±0.35 | 0.126±0.004 | 0.658±0.040 | 2.37 |
| GSCO-1A (B) | 850-2000 | 0.292±0.010 | 1.488±0.100 | 5.10±0.39 | 0.125±0.004 | 0.637±0.043 | 2.37 |
| GSCO-1A (B) | 2000-10000 | 0.262±0.009 | 1.359±0.083 | 5.18±0.36 | 0.112±0.004 | 0.582±0.035 | 2.37 |
| GSCO-1A (B) | >10000 | 0.189±0.006 | 1.211±0.070 | 6.41±0.42 | 0.081±0.003 | 0.519±0.030 | 2.37 |
| GSCO-7 (T) | 250-850 | 0.278±0.007 | 1.724±0.094 | 6.20±0.38 | 0.1026±0.0027 | 0.636±0.035 | 2.71 |
| GSCO-7 (T) | 850-2000 | 0.278±0.007 | 1.633±0.079 | 5.87±0.32 | 0.1027±0.0027 | 0.602±0.029 | 2.71 |
| GSCO-7 (T) | >2000 | 0.305±0.008 | 1.799±0.103 | 5.90±0.37 | 0.1124±0.0030 | 0.664±0.038 | 2.71 |
| GSLR-2 (T) | 250-850 | 0.256±0.008 | 1.404±0.088 | 5.48±0.38 | 0.094±0.003 | 0.514±0.032 | 2.76 |
| GSLR-2 (T) | 850-2000 | 0.230±0.008 | 1.262±0.068 | 5.49±0.35 | 0.084±0.003 | 0.462±0.025 | 2.76 |
| GSLR-2 (T) | 2000-10000 | 0.165±0.006 | 1.003±0.061 | 6.07±0.43 | 0.061±0.002 | 0.367±0.022 | 2.76 |
| GSLR-2 (T) | >10000 | 0.145±0.005 | 0.838±0.053 | 5.79±0.42 | 0.053±0.002 | 0.307±0.019 | 2.76 |
| GSLR-3 (T) | 250-850 | 0.178±0.006 | 0.000±0.000 | 0.00±0.0 | 0.064±0.002 | 0.000±0.000 | 2.81 |
| GSLR-3 (T) | 850-2000 | 0.202±0.009 | 0.000±0.000 | 0.00±0.0 | 0.073±0.003 | 0.000±0.000 | 2.81 |
| GSLR-3 (T) | 2000-10000 | 0.147±0.005 | 0.000±0.000 | 0.00±0.0 | 0.053±0.002 | 0.000±0.000 | 2.81 |
| GSLR-3 (T) | >10000 | 0.145±0.006 | 0.000±0.000 | 0.00±0.0 | 0.052±0.002 | 0.000±0.000 | 2.81 |
| GSLR-7 (B) | 250-850 | 0.240±0.008 | 0.000±0.000 | 0.00±0.0 | 0.104±0.003 | 0.000±0.000 | 2.35 |
| GSLR-7 (B) | 850-2000 | 0.245±0.008 | 0.000±0.000 | 0.00±0.0 | 0.106±0.003 | 0.000±0.000 | 2.35 |
| GSLR-7 (B) | 2000-10000 | 0.165±0.005 | 0.000±0.000 | 0.00±0.0 | 0.071±0.002 | 0.000±0.000 | 2.35 |
| GSLR-7 (B) | >10000 | 0.132±0.004 | 0.797±0.044 | 6.02±0.38 | 0.057±0.002 | 0.345±0.019 | 2.35 |

[1] Errors are 1σ uncertainties in analytical measurements (AMS, ICP); [2] Using basin-wide effective production rate (convolving hypsometric curves and Lal, 1991 for elevation/latitude correction without muon production); [3] Production factor is the ratio between the basin-wide effective production rate and sea level, >60° latitude production rate of 5.17 $^{10}$Be atoms yr$^{-1}$ (Bierman et al., 1996; Stone, 2000; Gosse and Stone, 2001); (B) Outlet rivers of the Great Smoky Mountains. (T) Tributary of Oconaluftee River (GSCO) and Little River (GSLR).

Table 5

*Interpretation of cosmogenic results of grain size test samples, Great Smoky Mountains*

| Sample name | Size fraction (μm) | $^{10}$Be model ε (m My$^{-1}$) | $^{26}$Al model ε (m My$^{-1}$) | $^{10}$Be Sediment generation rate (tons km$^{-2}$ yr$^{-1}$)[2] | $^{26}$Al Sediment generatio rate (tons km$^{-2}$ yr$^{-1}$)[2] |
|---|---|---|---|---|---|
| [1]GSCO-1 (B) | 250-850 | 28.0±6.1 | 29.8±6.7 | 76±16 | 80±18 |
| [1]GSCO-1 (B) | 850-2000 | 27.8±6.0 | 30.1±6.7 | 75±16 | 81±18 |
| [3]GSCO-1 (B) | >2000 | 28.4±6.1 | 29.0±6.5 | 77±17 | 78±18 |
| [1]GSCO-1A (B) | 250-850 | 24.7±3.2 | 27.3±3.8 | 67±9 | 74±10 |
| [1]GSCO-1A (B) | 850-2000 | 25.0±3.2 | 28.3±4.0 | 68±9 | 76±11 |
| [3]GSCO-1A (B) | 2000-10000 | 17.8±2.3 | 19.7±2.8 | 48±6 | 53±8 |
| [3]GSCO-1A (B) | >10000 | 29.0±3.7 | 27.2±3.8 | 78±10 | 73±10 |
| [1]GSCO-7 (T) | 250-850 | 30.5±6.6 | 28.3±6.3 | 82±18 | 76±17 |
| [1]GSCO-7 (T) | 850-2000 | 30.5±6.6 | 29.9±6.6 | 82±18 | 81±18 |
| [1]GSCO-7 (T) | >2000 | 27.9±6.0 | 27.1±6.1 | 75±16 | 73±16 |
| [1]GSLR-2 (T) | 250-850 | 33.4±4.2 | 35.2±4.9 | 90±11 | 95±13 |
| [1]GSLR-2 (T) | 850-2000 | 37.3±4.8 | 39.2±5.3 | 101±13 | 106±14 |
| [3]GSLR-2 (T) | 2000-10000 | 37.4±4.8 | 35.5±4.9 | 101±13 | 96±13 |
| [3]GSLR-2 (T) | >10000 | 42.7±5.5 | 42.6±6.0 | 115±15 | 115±13 |
| [1]GSLR-3 (T) | 250-850 | 49.1±6.3 | 00.0±0.0 | 133±17 | 00.0±0.0 |
| [1]GSLR-3 (T) | 850-2000 | 43.1±5.6 | 00.0±0.0 | 117±15 | 00.0±0.0 |
| [3]GSLR-3 (T) | 2000-10000 | 44.6±5.7 | 00.0±0.0 | 120±15 | 00.0±0.0 |
| [3]GSLR-3 (T) | >10000 | 45.3±5.9 | 00.0±0.0 | 122±16 | 00.0±0.0 |
| [1]GSLR-7 (B) | 250-850 | 30.2±3.9 | 00.0±0.0 | 82±10 | 00.0±0.0 |
| [1]GSLR-7 (B) | 850-2000 | 29.5±3.8 | 00.0±0.0 | 79±10 | 00.0±0.0 |
| [3]GSLR-7 (B) | 2000-10000 | 28.5±3.6 | 00.0±0.0 | 77±10 | 00.0±0.0 |
| [3]GSLR-7 (B) | >10000 | 41.5±5.3 | 41.8±5.7 | 112±14 | 113±15 |

[1] Erosion rates are calculated using the approach of Bierman and Steig, 1996, from normalized activities using basin-wide production rates (see text for discussion); [2] Sediment generation is calculated by multiplying erosion rate with basin area using density of 2.7 g cm$^{-3}$; [3]Erosion rates calculated using sampling site production rate (see text for discussion); (B) Outlet rivers of the Great Smoky Mountains; (T) Tributary of Oconaluftee River (GSCO) and Little River (GSLR). Erosion rates were calculated using sea-level, high-latitude $^{10}$Be production rate of 5.17 atoms g$^{-1}$ yr$^{-1}$ supported by data from Bierman et al. (1996), Stone (2000), and Gosse and Stone (2001). $^{10}$Be and $^{26}$Al model ε are calculated propagating 10% (1σ) uncertainty in production rate.

Table 6

*Interpretation of cosmogenic results from bedrock samples, Great Smoky Mountains*

| Sample name | $^{10}$Be model ε (m My$^{-1}$)[1] | $^{26}$Al model ε (m My$^{-1}$)[1] | $^{10}$Be Sediment generation rate (tons km$^{-2}$ yr$^{-1}$)[2] | $^{26}$Al Sediment generation rate (tons km$^{-2}$ yr$^{-1}$)[2] |
|---|---|---|---|---|
| GSC-3 | 15.8±3.4 | 15.6±3.5 | 43±9 | 42±10 |
| GSDV-1 | 22.6±4.9 | 22.5±5.1 | 61±13 | 61±14 |
| GSDV-2 | 40.8±5.3 | 00.0±0.0 | 110±14 | 00±0 |
| GSDV-3 | 48.0±6.1 | 00.0±0.0 | 130±17 | 00±0 |
| GSDV-4 | 30.9±4.1 | 00.0±0.0 | 84±11 | 00±0 |
| GSDV-6 | 4.7±0.6 | 00.0±0.0 | 13±2 | 00±0 |
| GSDV-7 | 32.4±4.1 | 00.0±0.0 | 88±11 | 00±0 |
| GSDV-8 | 37.7±4.9 | 32.3±4.3 | 102±13 | 87±12 |
| GSDV-10 | 34.2±4.4 | 00.0±0.0 | 92±12 | 00±0 |
| GSDV-11 | 23.0±2.9 | 23.8±3.2 | 62±8 | 64±9 |

[1] Erosion rates are calculated using the approach of Lal, 1988, from normalized activities using Lal, 1991 altitude/latitude correction function without muon production; [2] Sediment generation is calculated by multiplying erosion rate with basin area using density of 2.7 g cm$^{-3}$; Erosion rates were calculated using sea-level, high-latitude $^{10}$Be production rate of 5.17 atoms g$^{-1}$ yr$^{-1}$ supported by data from Bierman et al. (1996), Stone (2000), and Gosse and Stone (2001). $^{10}$Be and $^{26}$Al model ε are calculated propagating10% (1σ) uncertainty in production rate.

Table 7

*Interpretation of cosmogenic results of sediment samples (sand fraction)*

*Great Smoky Mountain*

| Sample name | $^{10}$Be model ε (m My$^{-1}$)[1] | $^{26}$Al model ε (m My$^{-1}$)[1] | $^{10}$Be sediment generation rate (tons Km$^{-2}$ yr$^{-1}$)[2] | $^{26}$Al sediment generation rate (tons Km$^{-2}$ yr$^{-1}$)[2] |
|---|---|---|---|---|
| GSRF-1 (T) | 19.3±4.2 | 20.1±4.5 | 52±11 | 54±12 |
| GSRF-2 (T) | 22.7±4.9 | 24.2±5.4 | 61±13 | 65±15 |
| GSRF-3 (T) | 16.9±3.7 | 18.1±4.1 | 46±10 | 49±11 |
| GSRF-5 (T) | 23.7±5.1 | 21.9±4.9 | 64 ±14 | 59±13 |
| GSRF-6 (T) | 25.0±5.4 | 28.0±6.2 | 68±15 | 76±17 |
| GSRF-7 (T) | 20.4±4.4 | 20.9±4.7 | 55±12 | 56±13 |
| GSRF-8 (T) | 27.2±5.9 | 36.2±8.3 | 73±16 | 98±22 |
| GSRF-9 (T) | 27.4±5.9 | 26.0±5.8 | 74±16 | 70±16 |
| GSRF-10 (T) | 24.6±5.3 | 24.7±5.6 | 66±14 | 67±15 |
| GSRF-11 (T) | 19.3±4.2 | 19.0±4.3 | 52±11 | 51±12 |
| GSRF-12 (B) | 24.8±5.4 | 30.0±6.7 | 67±14 | 81±18 |
| GSRF-13 (T) | 23.0±2.9 | 0.00±0.0 | 61±8 | 00±00 |
| GSCO-1 (B) | 28.0±6.1 | 29.8±6.7 | 76±16 | 80±18 |
| GSCO-1A (B) | 24.7±3.2 | 27.3±3.8 | 67±9 | 00±00 |
| GSCO-2 (B) | 30.1±6.5 | 31.8±7.1 | 81±18 | 86±19 |
| GSCO-3 (T) | 23.3±5.0 | 24.2±5.4 | 63±14 | 65±15 |
| GSCO-4 (T) | 35.1±7.6 | 39.5±9.2 | 95±20 | 107±25 |
| GSCO-5 (T) | 26.2±5.7 | 26.7±5.9 | 71±15 | 72±16 |
| GSCO-6 (T) | 20.2±4.4 | 20.4±4.6 | 55±12 | 55±12 |
| GSCO-7 (T) | 30.5±6.6 | 28.3±6.3 | 82±18 | 76±17 |
| GSLR-1 (B) | 24.8±5.4 | 23.3±5.2 | 67±14 | 63±14 |
| GSLR-2 (T) | 33.4±4.2 | 35.2±4.9 | 90±11 | 95±13 |
| GSLR-3 (T) | 49.1±6.3 | 0.00±0.0 | 133±17 | 00±00 |
| GSLR-4 (T) | 33.7±4.3 | 0.00±0.0 | 91±12 | 00±00 |
| GSLR-5 (T) | 25.6±3.3 | 0.00±0.0 | 69±9 | 00±00 |
| GSLR-6 (T) | 23.7±3.0 | 0.00±0.0 | 64±8 | 00±00 |
| GSLR-7 (B) | 30.2±3.9 | 0.00±0.0 | 82±10 | 00±00 |
| GSBC-1 (B) | 33.7±7.3 | 32.2±7.3 | 91±20 | 87±20 |
| GSBC-2 (B) | 33.0±7.1 | 37.6±8.4 | 89±19 | 102±23 |
| GSCS-1 | 36.9±7.9 | 37.1±8.2 | 99±21 | 100±22 |
| GSCS-2 | 17.4±3.8 | 18.3±4.1 | 47±10 | 49±11 |
| GSDC-1 (B) | 21.6±4.7 | 22.2±5.0 | 58±13 | 60±14 |
| GSLP-1 (B) | 31.8±6.9 | 32.2±7.2 | 86±19 | 87±19 |
| GSMP-1 (B) | 22.0±3.4 | 25.5±5.7 | 59±15 | 69±15 |
| GSWP-1 (B) | 31.0±6.7 | 34.6±7.7 | 84±18 | 93±21 |
| GSAC-1 (B) | 14.0±1.8 | 0.00±0.0 | 38±5 | 63±14 |
| GSPB-1 (B) | 17.8±2.4 | 0.00±0.0 | 48±6 | 00±00 |
| GSTM-1 (B) | 19.3±2.5 | 0.00±0.0 | 52±7 | 00±00 |
| GSNC-1 (B) | 19.1±2.5 | 0.00±0.0 | 52±7 | 00±00 |
| GSCA-1 (B) | 19.0±2.4 | 0.00±0.0 | 51±7 | 00±00 |

Table 7 (cont.)

| Sample name | $^{10}$Be model ε (m My$^{-1}$) | $^{26}$Al model ε (m My$^{-1}$) | $^{10}$Be sediment generation rate (tons Km$^{-2}$ yr$^{-1}$) | $^{26}$Al sediment generation rate (tons Km$^{-2}$ yr$^{-1}$) |
|---|---|---|---|---|
| GSFC-1 (B) | 19.4±2.5 | 0.00±0.0 | 52±7 | 00±00 |
| GSHC-1 (B) | 20.8±2.7 | 0.00±0.0 | 56±7 | 00±00 |
| GSEC-1 (B) | 17.1±2.2 | 0.00±0.0 | 46±6 | 00±00 |

[1] Erosion rates are calculated using the approach of Bierman and Steig, 1996, from normalized activities using basin-wide production rates; [2] Sediment generation is calculated by multiplying erosion rate with basin area and using density of 2.7 g cm$^{-3}$; (B) Outlet rivers of the Great Smoky Mountains; (T) Tributary of Oconaluftee River (GSCO), Raven Fork (GSRF), and Little River (GSLR). Erosion rates were calculated using sea-level, high-latitude $^{10}$Be production rate of 5.17 atoms g$^{-1}$ yr$^{-1}$ supported by data from Bierman et al. (1996), Stone (2000), and Gosse and Stone (2001), and normalized for latitude and elevation using nucleon only scaling of Lal (1991). $^{10}$Be and $^{26}$Al model ε are calculated propagating 10% (1σ) uncertainty.